Cell Metabolism

Article

Microbiota-derived lysophosphatidylcholine alleviates Alzheimer's disease pathology via suppressing ferroptosis

Graphical abstract

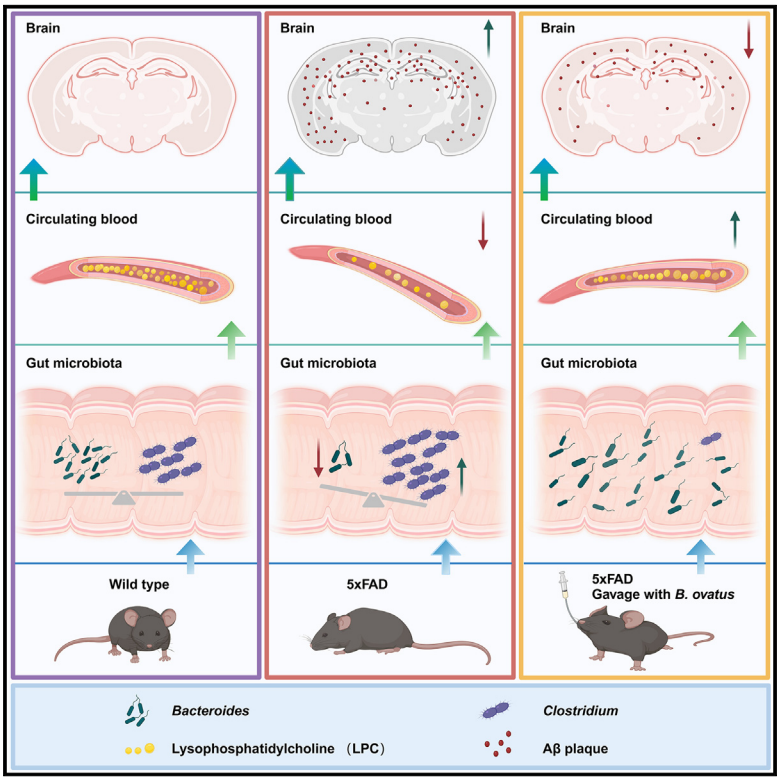

Highlights

- An imbalance of *Clostridium* and *Bacteroides* is a key feature linked to Aβ burden
- Supplementation of *B. ovatus* ameliorates AD pathologies
- Microbial-associated metabolite (LPC) ameliorates AD pathologies
- LPC inhibits ferroptosis through the orphan receptor GPR119 in an AD mouse model

Authors

Xu Zha, Xicheng Liu, Mengping Wei, ..., Yuping Xie, Wei Wang, Chen Zhang

Correspondence

liuxicheng@ccmu.edu.cn (X.L.), wangwei@ccmu.edu.cn (W.W.), czhang@ccmu.edu.cn (C.Z.)

In brief

Zha et al. reveal that dysbiosis, resulting from the loss of beneficial microbiota species, acts as a contributing factor in the pathogenesis of an AD mouse model. *B.ovatus*-triggered LPC-GPR119-ferroptosis axis ameliorates the symptoms of AD, showing potential for AD treatment.

Zha et al., 2025, Cell Metabolism *37*, 1–18
January 7, 2025
https://doi.org/10.1016/j.cmet.2024.10.006

CellPress

Cell Metabolism

CellPress
OPEN ACCESS

Article

Microbiota-derived lysophosphatidylcholine alleviates Alzheimer's disease pathology via suppressing ferroptosis

Xu Zha,[1,2,5] Xicheng Liu,[1,2,5,*] Mengping Wei,[1] Huanwei Huang,[1] Jiaqi Cao,[1] Shuo Liu,[1] Xiaomei Bian,[1] Yuting Zhang,[1] Fenyan Xiao,[1] Yuping Xie,[3] Wei Wang,[1,*] and Chen Zhang[1,2,4,6,*]

[1]School of Basic Medical Sciences, Beijing Key Laboratory of Neural Regeneration and Repair & Beijing Key Laboratory for Tumor Invasion and Metastasis, Beijing Laboratory of Oral Health, Capital Medical University, Beijing, China
[2]State Key Laboratory of Neurology and Oncology Drug Development, Nanjing, China
[3]National Center for Protein Sciences Beijing, State Key Laboratory of Proteomics, Beijing Proteome Research Center, Beijing Institute of Lifeomics, Beijing, China
[4]Chinese Institute for Brain Research, Beijing, China
[5]These authors contributed equally
[6]Lead contact
*Correspondence: liuxicheng@ccmu.edu.cn (X.L.), wangwei@ccmu.edu.cn (W.W.), czhang@ccmu.edu.cn (C.Z.)
https://doi.org/10.1016/j.cmet.2024.10.006

SUMMARY

Alzheimer's disease (AD) is a pervasive neurodegenerative disorder, and new approaches for its prevention and therapy are critically needed. Here, we elucidate a gut-microbiome-brain axis that offers actionable perspectives for achieving this objective. Using the 5xFAD mouse model, we identify increased *Clostridium* abundance and decreased *Bacteroides* abundance as key features associated with β-amyloid (Aβ) burden. Treatment with *Bacteroides ovatus*, or its associated metabolite lysophosphatidylcholine (LPC), significantly reduces Aβ load and ameliorates cognitive impairment. Mechanistically, LPC acts through the orphan receptor GPR119, inhibiting ACSL4 expression, thereby suppressing ferroptosis and ameliorating AD pathologies. Analysis of fecal and serum samples from individuals with AD also reveals diminished levels of *Bacteroides* and LPC. This study thus identifies a *B.ovatus*-triggered pathway regulating AD pathologies and indicates that the use of single gut microbiota, metabolite, or small molecule compound may complement current prevention and treatment approaches for AD.

INTRODUCTION

Alzheimer's disease (AD) is an incurable neurodegenerative disorder and the predominant form of dementia in elderly individuals, characterized by progressive cognitive impairment and a decline in cognitive function, which gradually prevents patients from performing daily activities.[1,2] To date, many hypotheses regarding the pathogenesis of AD have been proposed and experimentally validated.[1,3,4] The most widely accepted hypothesis regarding AD pathology is the amyloid cascade hypothesis. It posits that an imbalance between the production and clearance of β-amyloid (Aβ) in the brain is the initial trigger that eventually results in the degeneration of neurons and the development of dementia.[1] Misfolding and aggregation of Aβ peptides are recognized as hallmark features of AD and the initial events of AD development.[5] Therefore, the removal of aggregated Aβ from the brain is a major therapeutic strategy, and the effects of Aβ-targeted therapies, such as active and passive immunization and the administration of secretase inhibitors on sporadic forms of AD, have been extensively tested.[2,6] However, Aβ-targeted immunotherapies appear to be limited or ineffective in modifying the disease course of symptomatic AD.[2,6–8] Due to the limited efficacy of AD therapies, it is necessary to explore new pathophysiological mechanisms of the disease.

One such pathophysiological mechanism of interest involves the gut microbiota.[9] Multiple studies have reported gut microbial dysbiosis in both AD mouse models and individuals with AD and have found significant differences in gut microbiota abundance and diversity in these subjects compared with wild-type (WT) animals and control participants, respectively.[10–12] Notably, germ-free (GF) amyloidosis transgenic mice and antibiotic (ABX)-treated specific pathogen-free (SPF) AD model mice have significantly reduced Aβ plaque deposition,[13,14] transfer of the microbiota of amyloidosis model mice into GF amyloidosis transgenic mice increases cerebral Aβ pathology.[13] Although ABX treatments have shown promising effects in animal models, such measures may be logistically and ethically challenging to widely implement in humans. Gut-microbial-derived metabolites are one of focus to understand the mechanisms by which gut microbiota can affect brain physiology and pathology. A recent

Please cite this article in press as: Zha et al., Microbiota-derived lysophosphatidylcholine alleviates Alzheimer's disease pathology via suppressing ferroptosis, Cell Metabolism (2024), https://doi.org/10.1016/j.cmet.2024.10.006

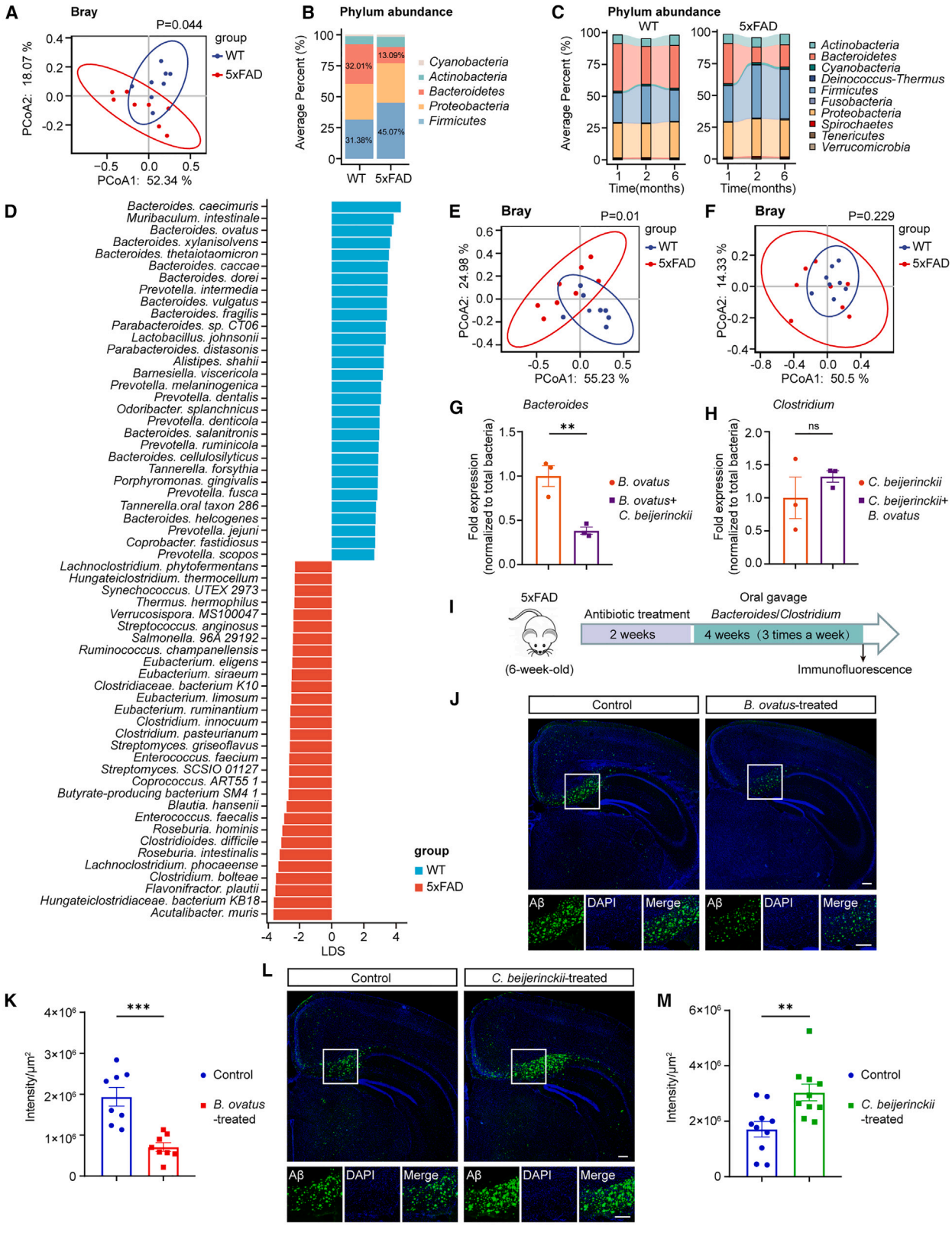

(legend on next page)

Please cite this article in press as: Zha et al., Microbiota-derived lysophosphatidylcholine alleviates Alzheimer's disease pathology via suppressing ferroptosis, Cell Metabolism (2024), https://doi.org/10.1016/j.cmet.2024.10.006

study on AD found that alterations in the composition of the gut microbiota result in the peripheral accumulation of microbial metabolites, which contributes to AD-associated neuroinflammation.[15] Furthermore, accumulating studies suggest that the gut microbiota and related metabolites regulate microglial maturation and function and impair oligodendrocyte maturation in normal mice and AD model mice.[16,17] These findings reveal that microbiota-derived metabolic products influence glial cell homeostasis and complex behaviors in AD. Nevertheless, the precise alterations in the composition of the gut microbiota that occur in AD are still not fully understood, the specific function of the gut microbiota and related metabolites in AD pathogenesis remain poorly defined, and the underlying mechanisms by which microbiota dysbiosis mediates gut-brain interactions are not well understood.

In this article, we investigated the correlation between gut microbiota and AD progression also established the gut-microbiome-brain axis in regulating AD symptoms. Specifically, employing mice model of AD, we observed a significant correlation between changes in gut microbiota composition and the development of AD pathology. Expansion of *Clostridium* and loss *Bacteroides* were key features associated with Aβ burden in this model. Remarkably, the delivery of *Bacteroides* and lysophosphatidylcholine (LPC) to AD model mice were found to reduce Aβ plaque load, rescue synaptic function, ameliorate cognitive impairment, decrease gliosis, and alleviate myelin degeneration. Lastly, we detected decreased abundance of *Bacteroides* in feces and reduced expression of LPC in serums from individuals with AD compared with healthy controls. Collectively, these findings suggest that *B. ovatus* and LPC interventions hold promise as potential therapeutic avenues for AD.

RESULTS

Gut microbiota dysbiosis occurs in mouse model of AD

To initially determine whether the microbiota is involved in Aβ deposition in the 5xFAD mouse model of AD, we treated 5xFAD mice with a broad-spectrum ABX cocktail to deplete the microbiota. Nanopore metagenomic sequencing analysis of fecal pellets showed that the total abundance of gut bacteria was profoundly reduced at the genus levels in ABX-treated mice (Figure S1A). The hippocampal Aβ plaque burden was significantly reduced in ABX-treated 5xFAD mice compared with vehicle controls (Figure S1B). Furthermore, the 5xFAD mice that received fecal microbiota from WT mice reduced Aβ deposition compared with that received microbiota from 5xFAD mice (Figure S1C). The transgenic mice with Aβ deposition exhibit impaired learning and working memory.[18] Given that ABX treatment ameliorated amyloid-related pathology, we evaluated its beneficial impacts on cognitive function in 5xFAD mice by using the novel object recognition (NOR), the Morris water maze (MWM) and the contextual fear conditioning (CFC) assay. We found that learning and memory impairments of 5xFAD mice were ameliorated after ABX treatment (Figures S1D–S1G). These data suggest that the microbiota regulates Aβ aggregation and ABX treatment reduces AD pathogenesis in 5xFAD mice.

Microbiota-related abnormalities, including disturbances in community composition, have been identified in individuals with AD, but the AD-associated microbial signature is not well defined.[10–12] To determine the features of the microbiota that affect AD pathogenesis and progression in 5xFAD mouse model, we conducted nanopore metagenomic sequencing of the fecal DNA of 2-month-old 5xFAD mice and age-matched WT mice. We investigated the taxonomic composition and diversity of the gut microbiota. The alpha diversity showed no significant differences between 5xFAD and WT mice (Figure S1H). However, the beta diversity of the gut bacteria was a notable disparity between 5xFAD and WT mice (Figures 1A and S1I).

The relative abundance of Bacteroidetes was significantly diminished and the relative abundance of Firmicutes was significantly elevated in 5xFAD mice in comparison with WT mice, while the levels of other phyla remained largely unchanged (Figures 1B, S1J, and S1K), consistent with previous studies.[15] Moreover, the abundance of Bacteroidetes and Firmicutes changed in opposite ways as the disease progressed in AD model mice (Figure 1C), and the same changes were also found at the genus level (Figure S1L). Of these differentially abundant genera, *Bacteroides* was more abundant in WT mice, and *Clostridium* and *Lachnoclostridium* were more abundant in AD model mice (Figures S1M and S1N). In comparison with WT mice, 5xFAD mice exhibited notable reductions in the overall abundance of multiple *Bacteroides* species, including *Bacteroides ovatus*, *Bacteroides dorei*, and *Bacteroides vulgatus*, and marked elevation in the abundance of *Clostridium* species, such as *Clostridium pasteurianum*, *Clostridium innocuum*, and *Clostridium beijerinckii* (Figure 1D). Notably, the difference in

Figure 1. Dysbiosis of the gut microbiota in 5xFAD mice manifests as increased *Clostridium* abundance and decreased *Bacteroides* abundance

(A) Principal coordinate analysis showing the species-level β-diversity of the gut microbiota in WT and 5xFAD mice.
(B) Stacked bar plots showing normalized abundance of microbiota taxa at phylum level.
(C) Average abundance changes of the gut microbiota at the phylum level in WT and 5xFAD mice at different ages (1, 2, and 6 months old).
(D) Linear discriminant analysis effect size (LEfSe) analysis of significant alterations at the species level.
(E and F) Beta diversity of gut microbial abundance including (E) or excluding (F) the species of *Bacteroides* and *Clostridium* in 2-month-old WT and 5xFAD mice.
(G and H) qPCR analysis of *Bacteroides* (G) and *Clostridium* (H) relative units in the feces of 5xFAD mice under the indicated treatment conditions.
(I) Experimental design framework for oral administration of bacteria.
(J and K) Example micrographs showing Aβ loads of brain slice (J) and quantitation of intensity (K), specifically in the subiculum region, in control and *B. ovatus*-treated 5xFAD mice. Scale bars: 200 μm.
(L and M) Representative micrographs (L) and quantitation (M) of Aβ plaques, in the subiculum of hippocampi, in 3-month-old control and *C. beijerinckii*-treated 5xFAD mice. Scale bars: 200 μm.
Data are presented as mean ± SEM. ns, not significant; $^{**}p < 0.01$, $^{***}p < 0.001$. (Unpaired t test in G, H, K and M,)
See also Figure S1.

Please cite this article in press as: Zha et al., Microbiota-derived lysophosphatidylcholine alleviates Alzheimer's disease pathology via suppressing ferroptosis, Cell Metabolism (2024), https://doi.org/10.1016/j.cmet.2024.10.006

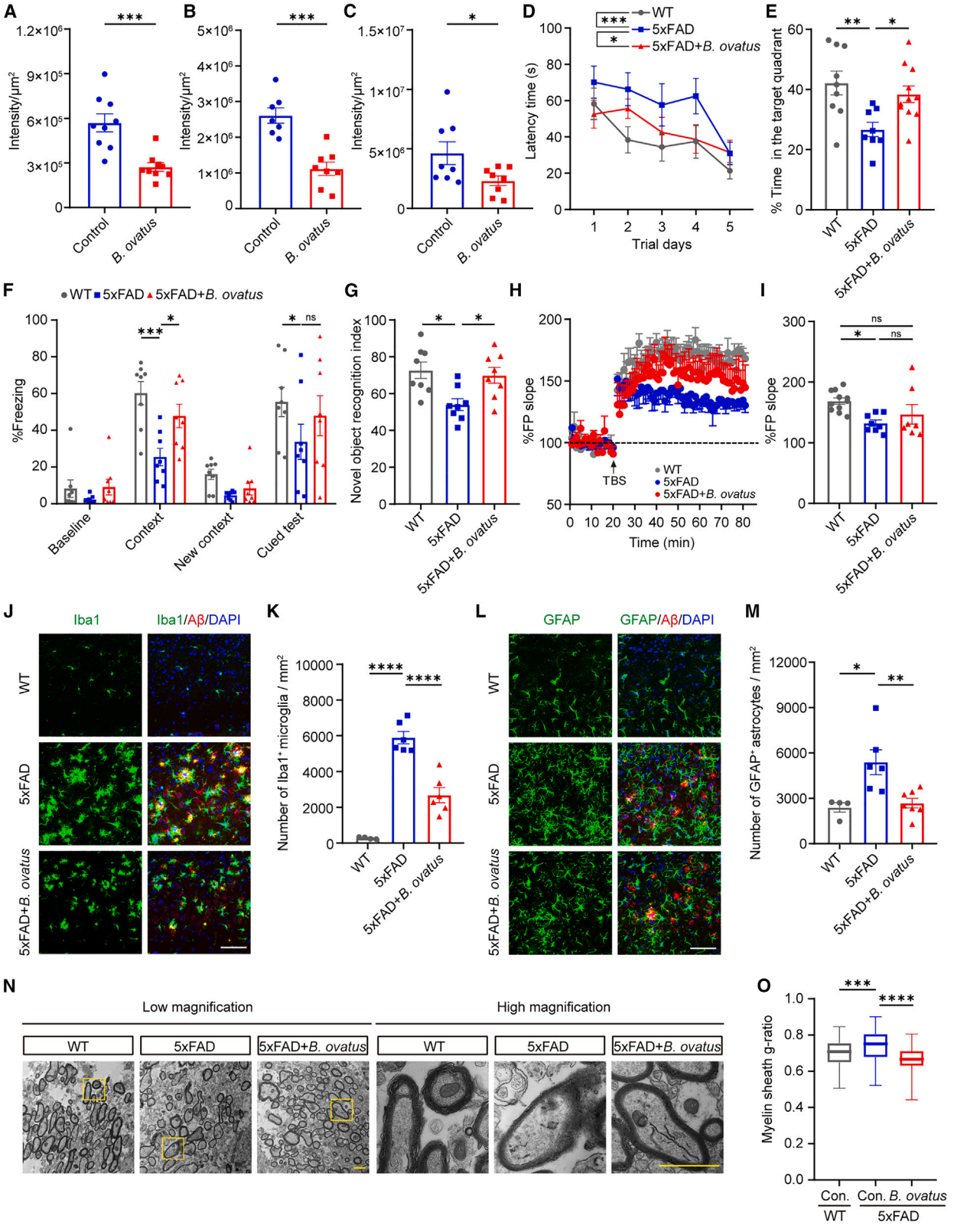

Figure 2. *B. ovatus* alleviates the pathological phenotypes of AD

(A–C) Quantification of Aβ intensity, specifically in the subiculum of hippocampi, in control and *B. ovatus*-treated 5xFAD mice at the ages of 2 (A), 6 (B), and 12 (C) months.

(legend continued on next page)

the composition of the gut microbiota between WT and 5xFAD mice was obvious when the sequences of *Clostridium* and *Bacteroides* species were included in principal coordinate analysis (PCoA) but not when they were specifically excluded from PCoA of all other bacterial species (Figures 1E and 1F). Furthermore, compared with WT mice, the abundance of *Bacteroides* species significantly decreased and the abundance of *Clostridium* species increased in 5xFAD mice during the progression of AD (Figures S1O and S1P). These results indicate that changes in *Clostridium* and *Bacteroides* diversity are the main drivers of the difference in the gut microbiota between WT and 5xFAD mice.

The above results suggest that the presence of *Clostridium* might reduce the abundance of *Bacteroides*. Therefore, we next tested whether *Clostridium* affects the colonization of *Bacteroides* species in AD mouse model. ABX-treated 5xFAD mice were colonized with *B. ovatus* with or without *C. beijerinckii*, and *C. beijerinckii* with or without *B. ovatus*. Consistent with our hypothesis, ABX-treated 5xFAD mice demonstrated a notable reduction in the abundance of *B. ovatus* in mice with *C. beijerinckii* colonization (Figure 1G). In contrast, the abundance of *C. beijerinckii* was not affected with *B. ovatus* colonization in ABX-treated 5xFAD mice (Figure 1H). Thus, increased abundance of *Clostridium* species, which is seen in 5xFAD mice, can antagonize the colonization of *Bacteroides* species.

In AD model mice and humans with neurodegenerative disease, AD pathology is associated with a loss of functional diversity within the *Bacteroides* genus.[19,20] To determine the role of *Bacteroides* in the AD-like phenotypes of 5xFAD mice, we treated 2-month-old 5xFAD mice by gavage with five human commensal *B. ovatus*, *B. vulgatus*, *B. dorei*, *Bacteroides thetaiotaomicron*, and *Bacteroides caccae* individually and then examined the effects of this treatment (Figure 1I). Aβ plaque formation in the hippocampal regions, one of the core features of the AD mouse model, was significantly reduced in *Bacteroides*-treated 5xFAD mice, except those treated with *B. thetaiotaomicron* and *B. caccae*, compared with untreated AD model mice, with *B. ovatus* resulting in the most significant impact in reducing Aβ plaques (Figures 1J, 1K, and S1Q–S1T). To determine the role of *Clostridium* in the development of AD-like phenotypes in 5xFAD mice, we treated 2-month-old 5xFAD mice with human commensal *C. beijerinckii*, *Clostridium acetobutylicum*, and *Clostridium sporogenes* by gavage and then examined the effects of this treatment by immunofluorescence analysis (Figure 1I). Remarkably, compared with untreated 5xFAD mice, *C. beijerinckii*-, *C. acetobutylicum*-, and *C. sporogenes*-treated 5xFAD mice displayed significantly increased Aβ deposition in the hippocampal regions (Figures 1L, 1M, S1U, and S1V). Collectively, these results indicate that specific *Clostridium* may play a role in AD pathogenesis, while *Bacteroides* may be protective.

Bacteroides ameliorates cognitive deficits in 5xFAD mice

Since the recent Aβ-immunotherapies mainly slow the progression of early AD,[6,8] we next proceeded to evaluate the potential of utilizing *Bacteroides* for the treatment of various stages of AD. To this end, we treated weaned, 4.5-month-old, and 12.5-month-old 5xFAD mice with *B. ovatus* through gavage and then examined the effects of those treatments (Figures S2A, S2C, and S2E). Notably, *B.-ovatus*-treated 5xFAD mice of different ages displayed significantly reduced Aβ plaque loads in hippocampal regions compared with untreated AD model mice (Figures 2A–2C, S2B, S2D, and S2F). Subsequently, we supplemented another mouse model of AD (3xTg-AD) with *B. ovatus*, which also reduced Aβ plaque loads (Figures S2G–S2I). These results indicate that *B. ovatus* may whole be effective in eliminating Aβ burdens in the brains of AD mice at different disease stages and in various mouse models of AD.

Given that *Bacteroides* ameliorated amyloid-related pathology, we evaluated its beneficial impacts on cognitive function in 5xFAD mice. We found that learning and memory impairments of 5xFAD mice were ameliorated after *B. ovatus* treatment in MWM, CFC, and NOR tests (Figures 2D–2G). Next, we performed fecal microbiota transplants (FMTs) from donors of the WT or 5xFAD mice into GF mice (Figure S2J). GF mice receiving FMT from 5xFAD feces (FMT-5xFAD) exhibited learning and memory deficits, which were ameliorated upon supplementation with *B. ovatus* (Figures S2K and S2L). Collectively, these studies demonstrate that *B. ovatus* treatment improved the cognitive functions in 5xFAD mice and FMT-5xFAD GF mice.

Since neurons exposed to Aβ peptides have demonstrated a decrease in the quantity of excitatory synapses.[21] To determine whether *B. ovatus* treatment could reverse the impairment of synaptic plasticity in hippocampal neuron of 5xFAD mice, we assessed long-term potentiation (LTP), a plasticity mechanism required for learning.[22] Compared with untreated 5xFAD mice, mice treated with *B. ovatus* showed a moderate reversal in the decrease in LTP at Schaffer collateral-CA1 synapses

(D and E) Graphs showing the latency time (seconds) to reach the platform in the acquisition phase (D) and the time spent in the target quadrant (%) in the probe trial (E) for mice from various groups in the MWM experiment.
(F) Quantification of the freezing behavior percentage in the CFC assay.
(G) Graph of the time percentage for interacting with the novel object during the testing phase of the NOR test.
(H and I) Plot of the mean field excitatory postsynaptic potential (fEPSP) slopes (H) and summary graph (I) of normalized field potentials (FP) slopes during the last 10 min (70–80 min).
(J) Representative fluorescence images, taken from the subiculum, showing co-staining of Iba1 (green), Aβ (red), and nuclei (blue). Scale bar: 100 μm.
(K) Quantification of Iba1-positive microglia cells.
(L) Typical fluorescence images illustrating co-staining of GFAP (green), Aβ (red), and nuclei (blue) in the subiculum region. Scale bar: 100 μm.
(M) Quantification of GFAP-positive astrocytes cells.
(N and O) Representative transmission electron microscopy (TEM) images of myelin (N) and quantitation of the g-ratio (r/R) of axons (O), which represents the thickness of the myelin sheath. Scale bars: 1 μm.
Data are presented as mean ± SEM. ns, not significant; $^{*}p < 0.05$, $^{**}p < 0.01$, $^{***}p < 0.001$, $^{****}p < 0.0001$. (Unpaired t test in A–C. Ordinary one-way ANOVA in E, G, I, K, M, and O. Two-way ANOVA in D and F).
See also Figure S2.

Please cite this article in press as: Zha et al., Microbiota-derived lysophosphatidylcholine alleviates Alzheimer's disease pathology via suppressing ferroptosis, Cell Metabolism (2024), https://doi.org/10.1016/j.cmet.2024.10.006

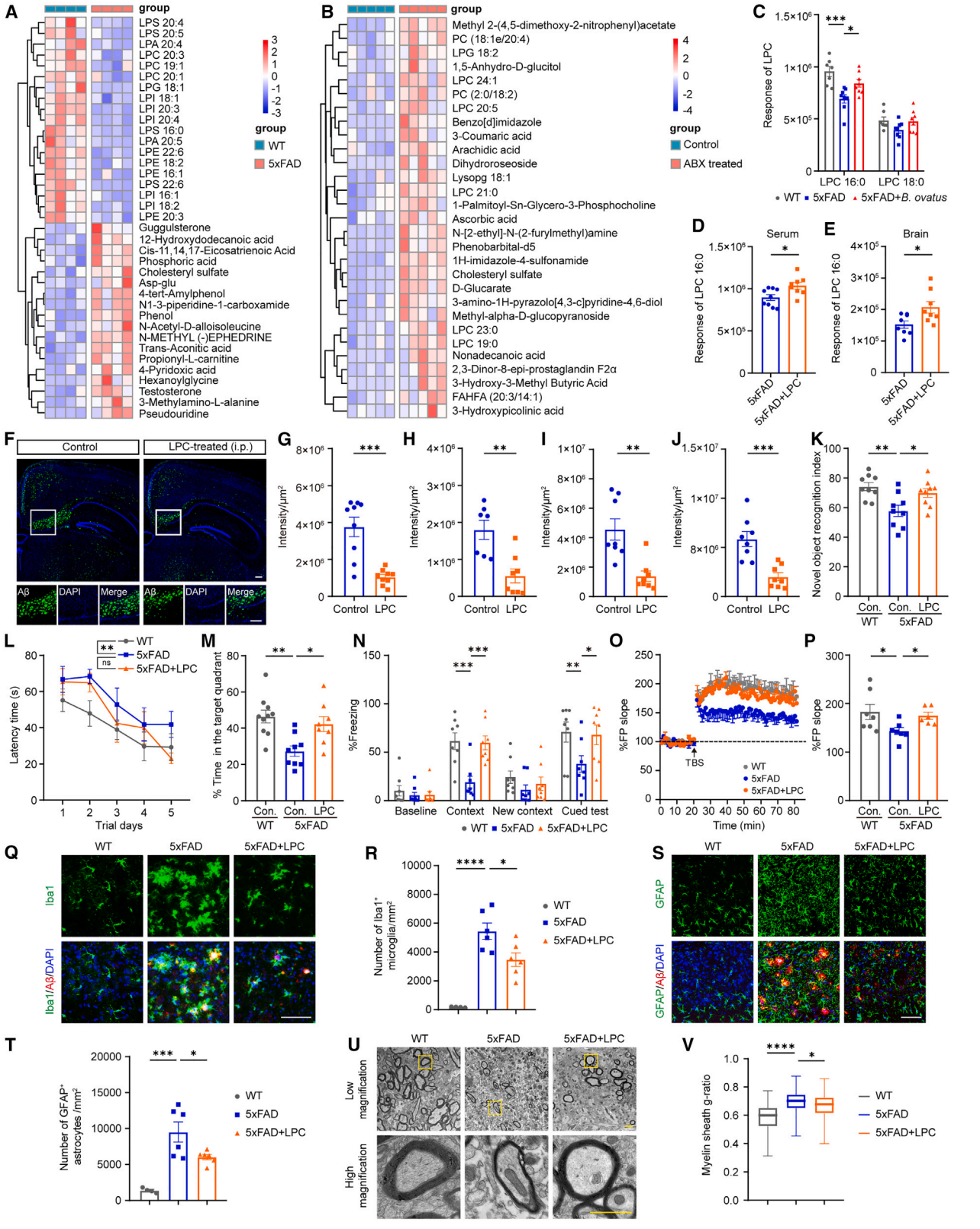

Figure 3. LPC in the serum correlates with the abundance of gut microbes and alleviates AD pathology

(A) Heatmap illustrating differential profile of serum metabolites in 2-month-old WT and 5xFAD mice.

(B) Heatmap showing upregulated serum metabolites in 2-month-old ABX-treated 5xFAD mice compared with the control group.

(legend continued on next page)

(Figures 2H, 2I, and S2M). Similarly, *B. ovatus* treatment prevented the decreases in the readily releasable pool (RRP) size and postsynaptic density (PSD) thickness in synaptic structure (Figures S2N–S2P). These observations demonstrate that *B. ovatus* treatment alleviated the deregulation of synaptic plasticity in 5xFAD mice. Furthermore, large numbers of lysosome-associated membrane protein 1 (LAMP1)-positive immature lysosomes accumulate around amyloid plaques leading to the exacerbation of synaptic impairment in AD.[23] *B. ovatus* treatment decreased the number of LAMP1-positive dystrophic neurites in 5xFAD mice (Figures S2Q and S2R), suggesting that *B. ovatus* treatment rescued synaptic dysfunction.

To determine whether the decreased Aβ burden observed in AD mouse model following *B. ovatus* treatment was accompanied with decreased gliosis, which accompanies Aβ deposition and is marked by an augmentation in the numbers of activated microglia and astrocytes surrounding amyloid plaques,[18,24,25] we treated 2-month-old AD model mice with *B. ovatus* and examined the effects of this treatment after 1 month. *B. ovatus* treatment ameliorated microglia-associated microgliosis, as assessed by the express level of ionized calcium-binding adapter molecule 1 (Iba1) (Figures 2J and 2K). Similar changes were observed in the abundance of glial fibrillary acidic protein (GFAP), a marker indicative of mature astrocytes, which were reduced by *B. ovatus* treatment (Figures 2L and 2M). Collectively, these results demonstrate that in addition to decreasing Aβ levels and deposition, *B. ovatus* treatment effectively reversed abnormalities in the quantity and activation of microglia and astrocytes, leading to a notable reduction in neuroinflammation in 5xFAD mice.

Since myelin degeneration resulting from myelin-forming oligodendrocyte dysfunction is an early event in AD that leads to cognitive deficits.[26,27] We next tested whether *B. ovatus* treatment would impact myelination and myelin repair. To confirm this, we used electron microscopy to characterize the myelin ultrastructure. 5xFAD mice showed uncompact myelin lamellae and degenerated sheaths. After *B. ovatus* treatment, the structure of myelin sheath recovered (Figures 2N and 2O). Together, these results demonstrate that in 5xFAD mice, *B. ovatus* ameliorated AD pathologies, including the improvement of cognitive performance and neuronal functions, a decrease in gliosis, and reduced myelin degeneration.

Microbially induced restoration of the levels of LPC ameliorates AD pathologies

Metabolites produced or induced to be generated by gut microorganisms may signal outside the gastrointestinal tract and regulate brain functions via the gut-brain axis.[28] To investigate the mechanism by which the gut microbiota alleviates amyloid-related pathology, we performed unbiased serum metabolomic profiling of 5xFAD mice and WT mice. Principal-component analysis (PCA) revealed that the metabolomic composition was striking differences between the two groups (Figure S3A). In total, 37 metabolites showed significant differences in abundance in AD mice compared with WT controls (Figure S3B). Those results revealed that the levels of lysolecithin family members, including lysophosphatidic acids (LPAs), LPC, lysophosphatidylethanolamines (LPEs), lysophosphatidylglycerols (LPGs), lysophosphatidylinositols (LPIs), and lysophosphatidylserines (LPSs), were notable decreased in 5xFAD mice compared with WT (Figure 3A), indicating that lysolecithin metabolism may be altered in 5xFAD mice.

Furthermore, we hypothesized that the abundance of gut bacterial species might correlate with the levels of the lysolecithin metabolites. To this end, we performed correlation analysis between the abundance of the *Clostridium* and *Bacteroides* species reported above and the levels of 18 lysolecithin metabolites. The levels of 17 lysolecithin metabolites, which were expressed at low levels in 5xFAD mice, exhibited a positive correlation with the abundance of *Bacteroides* and a negative correlation with the abundance of *Clostridium* species (Figure S3C). Next, we found that LPC levels were reduced in the sera of different ages 5xFAD mice, and we also found that the level of phosphatidylcholine (PC), which can be hydrolyzed to LPC,[29] was reduced (Figures S3D–S3I). More importantly, the serum LPC content and partial PC content were rescued in ABX-treated 2-month-old 5xFAD mice compared with untreated 5xFAD (Figure 3B). Notably, the LPC level, which was markedly decreased in 5xFAD mice compared with WT mice, was rescued by treatment with *B. ovatus* (Figure 3C). These results demonstrate that the gut microbiota regulates the levels of metabolites.

Plasma-derived LPCs are essential for normal brain growth and cognitive function,[30] and the concentrations of PCs and LPCs are diminished in individuals with AD.[31] Consistent with this, we observed lower LPC concentrations in 5xFAD mice

(C) Ultra-high-performance liquid chromatography-mass spectrometry (UPLC-MS)detection of LPC species (16:0 and 18:0) in serum of WT, 5xFAD mice, and 5xFAD mice treated with *B. ovatus*.
(D and E) The levels of LPC 16:0 in the serum (D) and brain (E) of 5xFAD mice treated with PBS or LPC, measured by UPLC-MS.
(F and G) Example micrographs of Aβ plaques (F) and quantitation of fluorescence intensity (G), specifically in the subiculum region, in 5xFAD mice treated with intraperitoneal injection of PBS (control) or LPC. Scale bars in (F): 200 μm.
(H–J) Quantification of Aβ intensity in the subiculum region, in control and LPC-treated 5xFAD mice at the ages of 2 (H), 6 (I), and 12 (J) months.
(K) Graph depicting the percentage of time that mice from different treatment groups spent interacting with the novel object.
(L and M) Graphs showing the latency time (seconds) in trial days (L) and duration of time (%) in the platform quadrant in probe test (M) for each group of mice in MWM experiment.
(N) Quantification of the percentage of freezing behavior exhibited by mice in the indicated group during the CFC assay.
(O and P) Plot of the mean fEPSP slopes (O) and summary graph (P) of normalized FP slopes during the 70th and 80th min in mice of indicated group.
(Q and R) Example micrographs (Q) and quantification (R) of Iba1-positive microglia cells. Scale bar: 100 μm.
(S and T) Typical fluorescence images (S) and quantification (T) illustrating GFAP-positive astrocytes cells. Scale bar: 100 μm.
(U and V) Typical TEM images of myelin (U) and quantitation of the g-ratio (r/R) of axons (V) per group. Scale bars: 1 μm.
Data are presented as mean ± SEM. ns, not significant; $*p < 0.05$, $**p < 0.01$, $***p < 0.001$, $****p < 0.0001$. (Unpaired t test in D, E, G–J, and P. Ordinary one-way ANOVA in C, K, M, R, T, and V. Two-way ANOVA in L and N).
See also Figure S3.

Please cite this article in press as: Zha et al., Microbiota-derived lysophosphatidylcholine alleviates Alzheimer's disease pathology via suppressing ferroptosis, Cell Metabolism (2024), https://doi.org/10.1016/j.cmet.2024.10.006

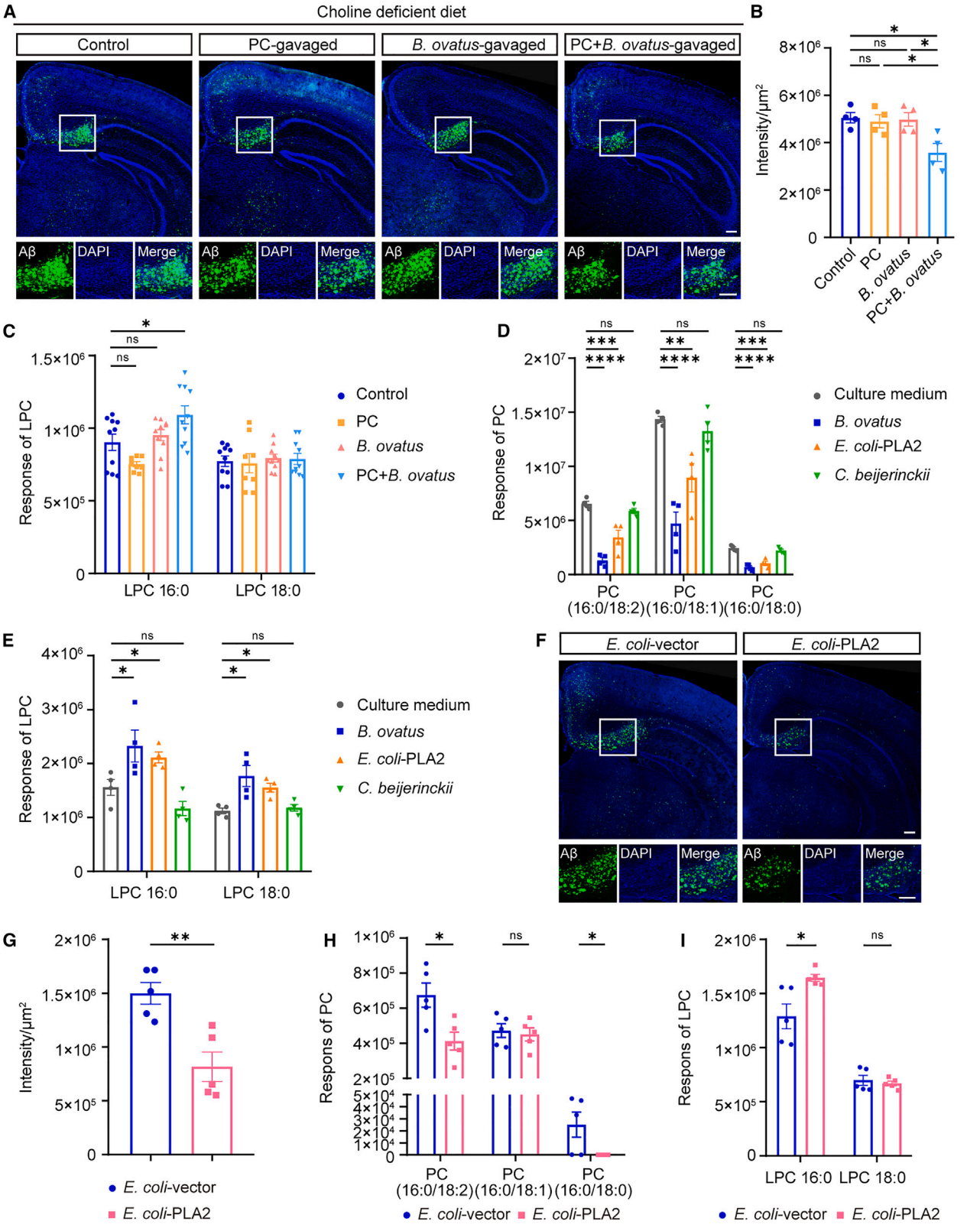

Figure 4. PLA2 of *B. ovatus* degrades PC to LPC

(A–C) Example micrographs of Aβ plaques (A), quantitative analysis of Aβ intensity in the subiculum (B) and the content of LPC in the serum (C) in 5xFAD mice treated with gavage of medium (control), PC, *B. ovatus*, or a combination of PC with *B. ovatus* under choline-deficient diet conditions.

(legend continued on next page)

Please cite this article in press as: Zha et al., Microbiota-derived lysophosphatidylcholine alleviates Alzheimer's disease pathology via suppressing ferroptosis, Cell Metabolism (2024), https://doi.org/10.1016/j.cmet.2024.10.006

than in WT mice. We wondered whether LPC treatment would be sufficient to reduce the Aβ load and rescue cognitive function in the AD model mice. To explore the link between microbial metabolites and AD symptoms in the AD mouse model, we treated 5xFAD mice with LPC via intraperitoneal (i.p.) injection. LPC treatment elevated the levels of LPC in both the serum and brain of 5xFAD mice (Figures 3D and 3E). Remarkably, the Aβ plaque loads in the hippocampal regions exhibited a significant decrease in LPC-treated 5xFAD mice compared with untreated AD model mice (Figures 3F and 3G). Furthermore, we supplemented 3xTg-AD with LPC, which also reduced Aβ loads (Figures S2G–S2I). Moreover, compared with untreated AD model mice, LPC-treated 25-day-old weaned, 4.5-month-old, and 12.5-month-old 5xFAD mice displayed markedly reduced Aβ aggregations (Figures 3H–3J, and S3J–S3O), similar to what was observed in *B. ovatus*-treated 5xFAD mice of different ages. These findings indicate that LPC has a protective role in the AD model mice.

Consistent with the reduction in amyloid load, we observed that performance was significantly improved in LPC-treated 5xFAD mice compared with untreated AD mice in NOR, MWM, and CFC tests (Figures 3K–3N), revealing that LPC significantly rescued cognitive function in 5xFAD mice. Interestingly, the decrease in LTP at Schaffer collateral-CA1 synapses showed remarkable amelioration in LPC-treated 6-month-old 5xFAD mice compared with untreated 5xFAD mice (Figures 3O, 3P, and S3P), and LPC treatment prevented the decrease in RRP size and PSD thickness in the 5xFAD mice (Figures S3Q–S3S). Furthermore, LPC-treated mice exhibited a decreased number of LAMP1-positive dystrophic neurites (Figures S3T and S3U), indicating the alleviation of deficits in neuron degeneration.

LPC treatment resulted in lower levels of Iba1 (Figures 3Q and 3R) and GFAP (Figures 3S and 3T), suggesting that LPC treatment decreased gliosis in 5xFAD mice. In addition, the myelin thickness was increased (Figures 3U and 3V), indicating that LPC treatment inhibited myelin degeneration. Thus, these results indicate that metabolites produced by the microbiota, like LPC, are essential for reducing amyloid deposition, thereby ameliorated synaptic dysfunction and gliosis while facilitated myelin nation and repair in AD mouse model.

PLA2 from *B. ovatus* hydrolyzes PC into LPC

On the basis of recent experimental evidence, higher PC intake is linked to a lower risk of developing dementia,[32] and similar associations between PC intake and cognitive performance have been reported.[33] In contrast, treatment with PC via i.p. injection failed to reduce the Aβ plaque load in AD model mice (Figures S4A and S4B). To explain the reduction in the efficacy of i.p. PC in AD mice, 5xFAD mice were administered for 2 weeks with ABX as described above and administered *B. ovatus* + PC or PC only via oral gavage. Notably, compared with control and PC-treated alone 5xFAD mice, *B. ovatus* + PC-treated 5xFAD mice displayed a notable decrease in the accumulation of Aβ plaques in the hippocampal regions (Figures S4C–S4E). We next sought to further determine PC function and the features of gut microbiota that are required for PC hydrolysis. To carry out this goal, we fed 5xFAD mice with choline-deficient diet and administered PC, *B. ovatus*, or *B. ovatus* + PC via oral gavage. We found that under choline deficiency and ABX treatment, *B. ovatus* + PC treatment effectively reduced the accumulation of Aβ plaques, whereas *B. ovatus*- or PC-treatments alone showed weakly reduction of Aβ deposition (Figures 4A and 4B). Similarly, the serum LPC level of 5xFAD mice was elevated after *B. ovatus* + PC treatment, confirming *B. ovatus* as a necessary driver (Figure 4C). Further, we demonstrated that the culture supernatant of *B. ovatus* was insufficient to reduced Aβ loads (Figures S4F and S4G). These results indicate that the effect of PC in modulating Aβ accumulation dependent on *B. ovatus* activity.

LPC is a metabolite of PC, specifically as a product of PC hydrolysis by phospholipase A2 (PLA2).[29] We hypothesized that the PLA2 from *B. ovatus* might play a crucial role in the hydrolysis of PC into LPC. To test this, we first cloned the *Pla2* gene from *B. ovatus* into the pET-21b (+) vector and heterologous overexpressed in *E. coli* BL21(*E. coli*-PLA2) and monitored the production of the hydrolysis halos by *B. ovatus*, *E. coli*-PLA2 or *C. beijerinckii* on egg yolk agar plates, serving as an indicator of PLA2 activity. A white precipitate ring forms on plates around the previously inoculated with *B. ovatus* and *E. coli*-PLA2, while those inoculated with *C. beijerinckii* did not (Figure S4H). Subsequently, we incubated *B. ovatus*, *E. coli*-PLA2 or *C. beijerinckii* with PC in culture medium. Quantitative analysis showed that *B. ovatus* and *E. coli*-PLA2 transformed PC into LPC, as compared with the controls (Figures 4D and 4E). In contrast, PC was not degraded by *C. beijerinckii*. These results demonstrate that *B. ovatus* are involved in PC metabolism and generated metabolites LPC.

Next, we supplemented *E. coli*-PLA2 into 5xFAD mice to assess whether *E. coli*-PLA2 could reduce Aβ load. The results showed that the hippocampal Aβ plaque burden was significantly reduced in *E. coli*-PLA2-treated 5xFAD mice compared with vehicle controls (Figures 4F and 4G). Furthermore, the serum PC levels in the *E. coli*-PLA2-treated 5xFAD mice were significantly lower than those in the vehicle controls (Figure 4H). Conversely, the serum LPC levels in the *E. coli*-PLA2-treated 5xFAD mice were significantly increased (Figure 4I). The above results support our hypothesis that PLA2 from *B. ovatus* can hydrolyze PC into LPC, then reducing the Aβ plaque load in 5xFAD mice.

LPC alleviates AD pathologies through suppressing ferroptosis

We next investigated the mechanisms underlying the effect of LPC on AD development. To this end, we examined the reactions

(D and E) Graphs showing the degradation of PC (D) and production of LPC (E) by culture medium, *B. ovatus*, *E. coli*-PLA2, or *C. beijerinckii*, as detected by UPLC-MS.

(F and G) Representative photomicrographs (F) and assessment (G) of Aβ deposits in the subiculum of hippocampi in 5xFAD mice with *E. coli*-vector and *E. coli*-PLA2 treatment.

(H and I) Concentration of PC (H) and LPC (I) in the serum of the *E.coli*-vector- and *E.coli*-PLA2-treated 5xFAD mice, as detected by targeted UPLC-MS.

Data are presented as mean ± SEM. ns, not significant; $^{*}p < 0.05$, $^{**}p < 0.01$, $^{***}p < 0.001$, $^{****}p < 0.0001$. (Unpaired t test in G–I. Ordinary one-way ANOVA in B–E). Scale bars: 200 μm. See also Figure S4.

Please cite this article in press as: Zha et al., Microbiota-derived lysophosphatidylcholine alleviates Alzheimer's disease pathology via suppressing ferroptosis, Cell Metabolism (2024), https://doi.org/10.1016/j.cmet.2024.10.006

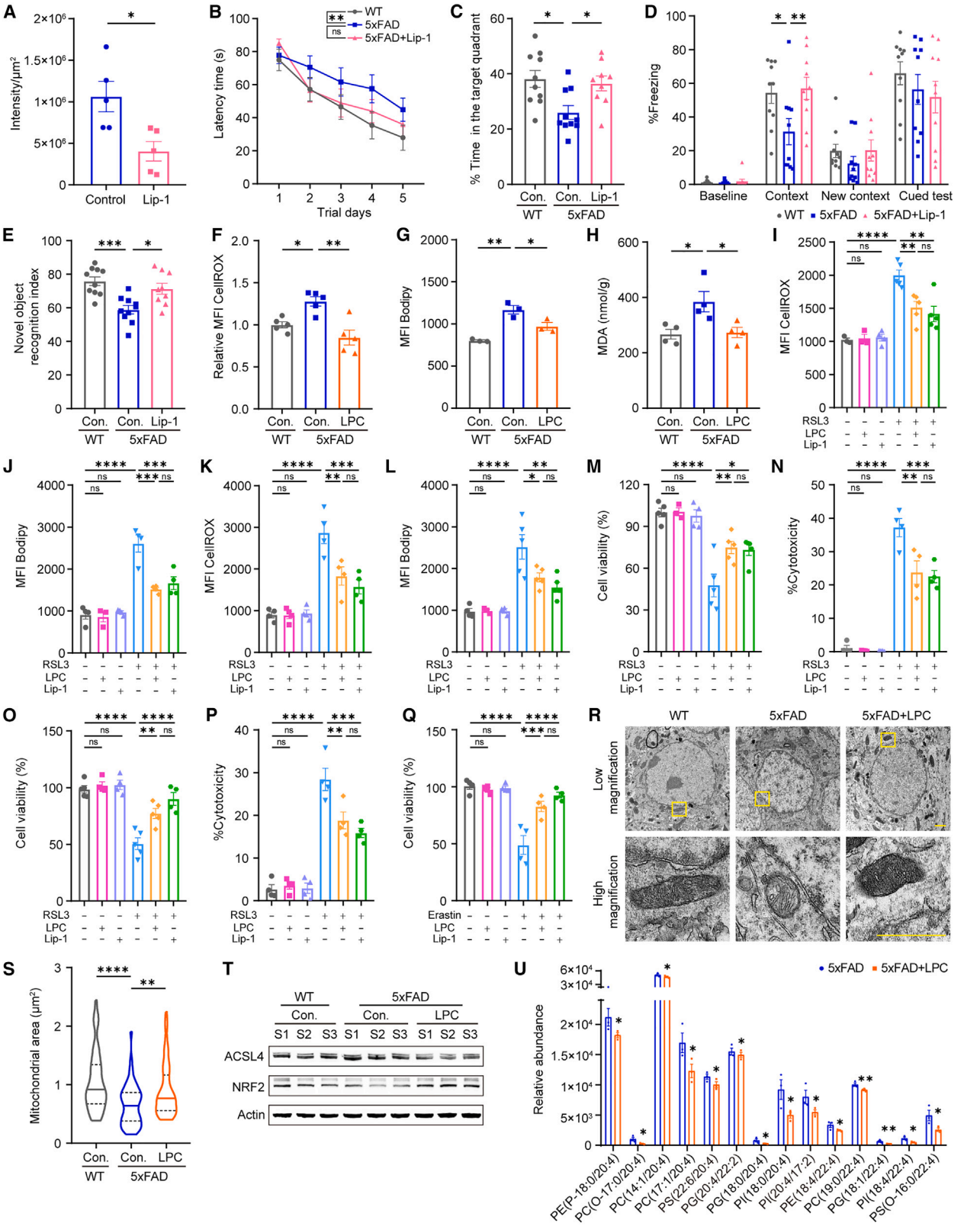

(legend on next page)

of distinct cell types in the hippocampus of 5xFAD mice to LPC treatment. Neuronal and glial cells (microglial cell, astrocyte, and oligodendrocyte)-enriched brain cell suspensions from LPC-treated mice, LPC-untreated 5xFAD mice and control mice were subjected to single-cell RNA sequencing (RNA-seq) with Smart-seq2 (Figure S4I). A total of seven groups of brain cells, comprising neurons, oligodendrocytes, microglia, and astrocytes were identified (Figure S4J). Neurons from 5xFAD mice exhibited upregulation of genes that were enriched in Kyoto Encyclopedia of Genes and Genomes (KEGG) pathways associated with various processes, including oxidative phosphorylation, reactive oxygen species (ROS) in chemical carcinogenesis, thermogenesis, and AD, and these pathways are closely linked to ferroptosis and neurodegeneration[34] (Figure S4K). Significantly, the administration of LPC treatment resulted in a decrease in the expression of genes enriched in these KEGG pathways in neurons (Figure S4K). Transcriptional changes were also found in the brain microglia, astrocytes and oligodendrocytes, and genes that were regulated in those cells were mainly involved in ferroptosis (Figures S4L–S4N).

To determine whether the inhibitory effect of LPC on AD pathologies is mediated through ferroptosis, we administered liproxstatin-1 (Lip-1, an inhibitor of ferroptosis) via i.p. injection to 5xFAD mice, and parameters of AD pathology were monitored. Strikingly, consistent with LPC treatment, following Lip-1 administration, 5xFAD mice exhibited a significant decrease in Aβ plaque loads relative to untreated 5xFAD mice (Figures 5A and S5A). Furthermore, learning and memory impairments of 5xFAD mice were ameliorated after Lip-1 administration in MWM, CFC, and NOR tests (Figures 5B–5E). Ferroptosis is a form of cell death driven by iron-dependent lipid peroxidation.[35] The levels of ROS and lipid peroxidation were significantly elevated in hippocampi living cells and tissues from 5xFAD mice compared with WT mice, which were significantly reduced after treatment with LPC and *B. ovatus* (Figures 5F–5H and S5B–S5D). Similarly, with LPC or Lip-1 treatment, the elevated levels of ROS and lipid peroxidation were also restored in RSL3-induced neuronal and glial cell lines (Figures 5I–5L and S5E–S5I). Ferroptotic cell death induced by RSL3 or erastin was also restored by LPC or Lip-1 (Figures 5M–5Q and S5J–S5L). Furthermore, we found smaller, ruptured mitochondria (the most prominent characteristic of ferroptosis)[36] in the perinuclei of hippocampal neurons in 5xFAD mice. The mitochondrial structure and area were reversed after LPC and *B. ovatus* treatment (Figures 5R, 5S, S5M, and S5N). Other forms of cell death such as apoptosis, pyroptosis, and autophagy were significantly elevated in 5xFAD mice compared with WT mice, and LPC treatment failed to rescue these death processes (Figures S5O and S5P). These results suggest that the regulatory effect of LPC may be dependent on the ferroptosis.

Inhibition of ACSL4-dependent ferroptosis by LPC requires GPR119

We next investigated the mechanisms for LPC-mediated ferroptosis inhibition. To this end, we performed RNA-seq of LPC-treated cells under RSL3 induction. LPC induced marked changes in global gene expression (Figure S5Q). Among the genes that were downregulated by LPC was that encoding the protein ACSL4, an essential regulator of ferroptosis.[37] Furthermore, real-time PCR and western blotting analysis revealed a downregulation of ACSL4 expression following LPC treatment (Figures 5T, S5R, and S5S).

Phospholipid-bound polyunsaturated fatty acids (PL-PUFAs), as principal substrates for lipid peroxidation, are intricately involved in the ferroptotic process.[34,38] Their assimilation into PLs requires ACSL4, a pivotal step in the execution of ferroptosis.[39] To validate whether LPC inhibits ACSL4-induced lipid peroxidation, we performed untargeted lipidomic analysis in the hippocampus tissues of WT mice, 5xFAD mice and LPC-treated 5xFAD mice. PL-PUFAs are significantly upregulated in the hippocampus tissues of 5xFAD mice compared with WT mice (Figure S5T), while LPC treatment significantly reversed the change in the profile of PL-PUFAs (Figure S5U). Notably, LPC treatment substantially lowered phosphatidylethanolamines-arachidonoyl (PE-AAs), PE-adrenoyl (AdAs), and PC-PUFAs (Figure 5U), which have been confirmed as the principal PL-PUFAs most closely linked to increased ferroptosis susceptibility.[34,38,40] Additionally, LPC administration did not change the expression levels of the FSP1 and MBOAT1 proteins in 5xFAD mice, as compared with untreated 5xFAD mice

Figure 5. LPC suppresses ferroptosis

(A) Quantitative analysis of Aβ intensity in the subiculum, within control and Lip-1-treated 5xFAD mice.
(B–E) Graphs showing the latency time (B) and percent of time searching in target quadrant (C) in the MWM test, the freezing behavior in the CFC experiment (D) and the percentage of time for interacting with the novel object in the NOR test (E) by WT, 5xFAD mice, and 5xFAD + Lip-1 mice.
(F) The quantitative data of relative mean fluorescence intensity (MFI) determined by CellROX-labeled ROS in live hippocampal cells from mice in the indicated groups.
(G) Flow cytometry analysis of lipid peroxidation in single cells isolated from the hippocampi of WT, 5xFAD mice, and LPC-treated 5xFAD mice using BODIPY 581/591 C11 as a marker.
(H) Malondialdehyde (MDA) content in the hippocampi of mice.
(I and J) Flow cytometry analysis showing ROS (I), lipid peroxidation (J) in SH-SY5Y cells after RSL3 treatment with or without LPC.
(K and L) ROS (K) and lipid peroxidation (L) levels in HT22 cells following RSL3 treatment, with or without LPC and Lip-1 supplementation.
(M and N) RSL3 induced cell viability (M) and LDH release (N) in SH-SY5Y cells with or without LPC treatment.
(O and P) RSL3 induced cell viability (O) and LDH release (P) in HT22 cells with or without LPC treatment.
(Q) HT22 cell viability following erastin treatment and LPC or Lip-1 supplementation.
(R and S) Exemplary TEM images (R) and quantitation (S) of the mitochondrial area in the perinuclear.
(T) Western blotting showing the protein levels of ACSL4 and NRF2 expression in hippocampi of mice.
(U) Quantification of significantly decreased PL-AAs and PL-AdAs in the hippocampi of LPC-treated 5xFAD mice compared with 5xFAD mice, as indicated.
Data are presented as mean ± SEM. ns, not significant; $^{*}p < 0.05$, $^{**}p < 0.01$, $^{***}p < 0.001$, $^{****}p < 0.0001$. (Unpaired t test in A and U. Ordinary one-way ANOVA in C, E–Q, and S. Two-way ANOVA in B and D).
See also Figure S5.

Please cite this article in press as: Zha et al., Microbiota-derived lysophosphatidylcholine alleviates Alzheimer's disease pathology via suppressing ferroptosis, Cell Metabolism (2024), https://doi.org/10.1016/j.cmet.2024.10.006

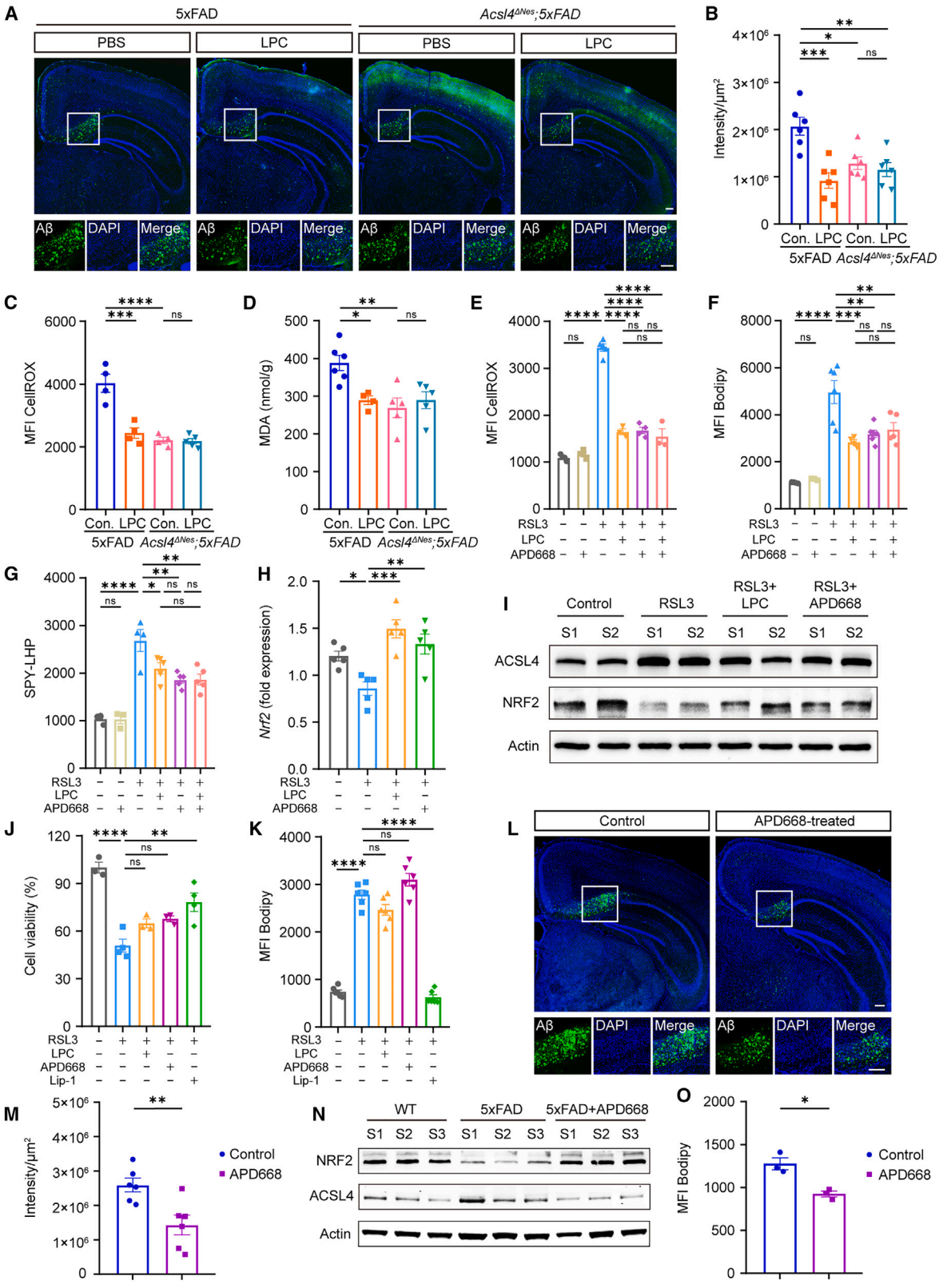

Figure 6. LPC attenuates ferroptosis by regulating NRF2-ACSL4 axis through receptor GPR119

(A and B) Representative micrographs showing Aβ plaques of brain slice (A) and quantitation of Aβ intensity (B), particularly in the subiculum, in 5xFAD and *Acsl4*$^{\Delta Nes}$*;5xFAD* mice treated with PBS and LPC.

(legend continued on next page)

Please cite this article in press as: Zha et al., Microbiota-derived lysophosphatidylcholine alleviates Alzheimer's disease pathology via suppressing ferroptosis, Cell Metabolism (2024), https://doi.org/10.1016/j.cmet.2024.10.006

(Figure S5P), despite these proteins being confirmed as inhibitors of ferroptosis.[38,41] Although LPC treatment upregulated the expression of GPX4 in 5xFAD mice, LPC continued to inhibit ferroptosis and alleviate AD pathologies in *Gpx4*-deficient AD model mice and *Gpx4* KO neuronal cell line (Figures S6A–S6G).

We therefore hypothesized that the reduction of ACSL4 may be important for LPC-mediated inhibition of AD pathology. To test this, although *Acsl4* knockout (KO) was not as efficient as LPC, the lipid peroxidation of neuronal and glial cells under the combinational treatment were comparable to that under LPC treatment (Figures S6H and S6I). However, overexpression of *Acsl4* was sufficient to increase RSL3-induced lipid peroxidation and was resistant to LPC treatment (Figures S6J and S6K). Furthermore, the levels of Aβ plaque load, ROS and lipid peroxidation were reduced in *Acsl4*-deficient AD model mice, and those levels did not show further reduction after LPC treatment (Figures 6A–6D and S6L). These data indicate that ASCL4 could be a potential target downstream of LPC.

We next sought to determine the mechanisms by which LPC inhibits ACSL4 expression. Orphan receptor GPR119 has been previously identified as the receptor for LPC.[42] To test this, we exposed *Gpr119* KO and WT neuronal and glial cell lines to LPC. Whereas LPC reduced the levels of ROS and lipid peroxidation induced by RSL3 in WT cells, *Gpr119* KO cells were resistant to LPC treatment (Figures S6M–S6R). Furthermore, the ROS and lipid peroxidation levels in neuronal and glial cells under RSL3 treatment were decreased by APD668, a clinical-stage agonist of GPR119,[42] and these levels did not show further reduction in cells treated with a combination of LPC and APD668 (Figures 6E–6G and S6S–S6V). Consistently, the levels of ACSL4 were diminished upon treatment with APD668 (Figure S6W). The data indicate that the resistance to ferroptosis mediated by LPC depends on the GPR119-ACSL4 axis.

We thus considered potential mechanisms underlying the GPR119-regulated expression of ACSL4. Because NRF2 is a well-known transcription factor that plays a key role in ferroptosis, capable of directly or indirectly regulating ferroptosis-related proteins.[43] NRF2 suppressed the expression of ACSL4 in mouse hippocampal neuronal cell lines.[44] We explored whether NRF2 inhibition mediates the effect of GPR119 on ACSL4 expression. We first verified LPC or APD668 treatment increases the transcription and translation levels of the *Nrf2* gene (Figures 6H and 6I), thus suggesting NRF2 as a possible mediator of the effect of LPC. To verify this finding, we then treated *Nrf2*-deficient neuronal cell lines with LPC or APD668. *Nrf2* deficiency attenuated the inhibitory effect of LPC and APD668 on RSL3-induced ferroptosis compared with the control group (Figures 6J and 6K). By contrast, Lip-1 still suppressed ROS and lipid peroxidation in the absence of *Nrf2*. Furthermore, immunoblot analysis revealed a decreased expression of NRF2 in the hippocampal tissues of 5xFAD mice relative to controls, with LPC treatment effectively reinstating NRF2 protein levels (Figure 5T). These results indicate that LPC engages GPR119 and subsequently antagonizes cellular ferroptosis through the regulation of the NRF2-ACSL4 axis.

To further investigate whether the activation of GPR119 explains the inhibition of Aβ deposition in an LPC-treated AD mouse model, we administered APD668 orally once every 2 days. Administration of APD668 reduced Aβ deposition in the brain of 5xFAD mice (Figures 6L, 6M, S6X, and S6Y). Additionally, APD668 delivery increased the expression of NRF2 while decreasing the expression of ACSL4 (Figure 6N), and the decrease was accompanied by a reduction in the severity of lipid peroxidation (Figure 6O). Collectively, our results illustrate that LPC regulates NRF2-ACSL4 axis by targeting GPR119, and thereby ameliorating AD pathologies by inhibiting ferroptosis. Therefore, GPR119 activation is a potential strategy for reducing brain Aβ deposition and alleviating AD symptoms.

Gut microbiota and clinical AD

To elucidate the changes in gut microbiota and LPC levels in humans, we collected fecal and serum samples from individuals with AD and age-matched control donors. At the phylum and genus levels, we found a decrease in the abundance of Bacteroidetes and *Bacteroides* in the fecal samples of individuals with AD, while the abundance of Firmicutes and *Clostridium* was slightly elevated in AD (Figures S7A–S7C). Notably, among the healthy control donors, *B. ovatus* exhibited the highest abundance in the fecal samples (Figures 7A and 7B). Subsequently, we performed lipidomic analysis on the serum samples of individuals with AD and age-matched control donors. In terms of metabolites, there was a significant reduction in LPC concentration in the sera of individuals with AD (Figures 7C, 7D, and S7D–S7F).

DISCUSSION

Recent studies have identified a key role for the gut microbiota in multiple phenotypes associated with neurological diseases, including AD, Parkinson's disease (PD), and amyotrophic lateral sclerosis (ALS).[45–50] We found that prolonged administration of ABX severely disrupted the gut microbiota composition, leading

(C and D) The effect of LPC on ROS (C) and lipid peroxidation (D) in *Acsl4*$^{\Delta Nes}$*;5xFAD* mice, as evaluated by measuring the MFI of CellROX and the level of MDA.
(E–G) Flow cytometry assessment of RSL3-induced ROS (E), lipid oxidation (F), and lipid hydroperoxides (G) in control and LPC or APD668-treated SH-SY5Y cells.
(H and I) The mRNA levels (H) and protein levels (I) of NRF2 in SH-SY5Y cells under the indicated treatment.
(J and K) Cell viability (J) and lipid peroxidation (K) of *Nrf2* knockout SH-SY5Y cell assessing under RSL3-induced conditions with or without LPC, APD668, and Lip-1.
(L and M) Example micrographs (L) and quantitation (M) of Aβ plaques particularly in the subiculum of control and APD668-treated 5xFAD mice.
(N) Western blotting showing the protein levels of ACSL4 and NRF2 in the hippocampi of mice per group.
(O) Lipid oxidation as determined by BODIPY 581/591 C11 in hippocampal cells from control and APD668-treated 5xFAD mice.
Data are presented as mean ± SEM. ns, not significant; $^{*}p < 0.05$, $^{**}p < 0.01$, $^{***}p < 0.001$, $^{****}p < 0.0001$. (Ordinary one-way ANOVA in B–H, J, and K. Unpaired t test in M and O).
Scale bars: 200 μm. See also Figure S6.

Please cite this article in press as: Zha et al., Microbiota-derived lysophosphatidylcholine alleviates Alzheimer's disease pathology via suppressing ferroptosis, Cell Metabolism (2024), https://doi.org/10.1016/j.cmet.2024.10.006

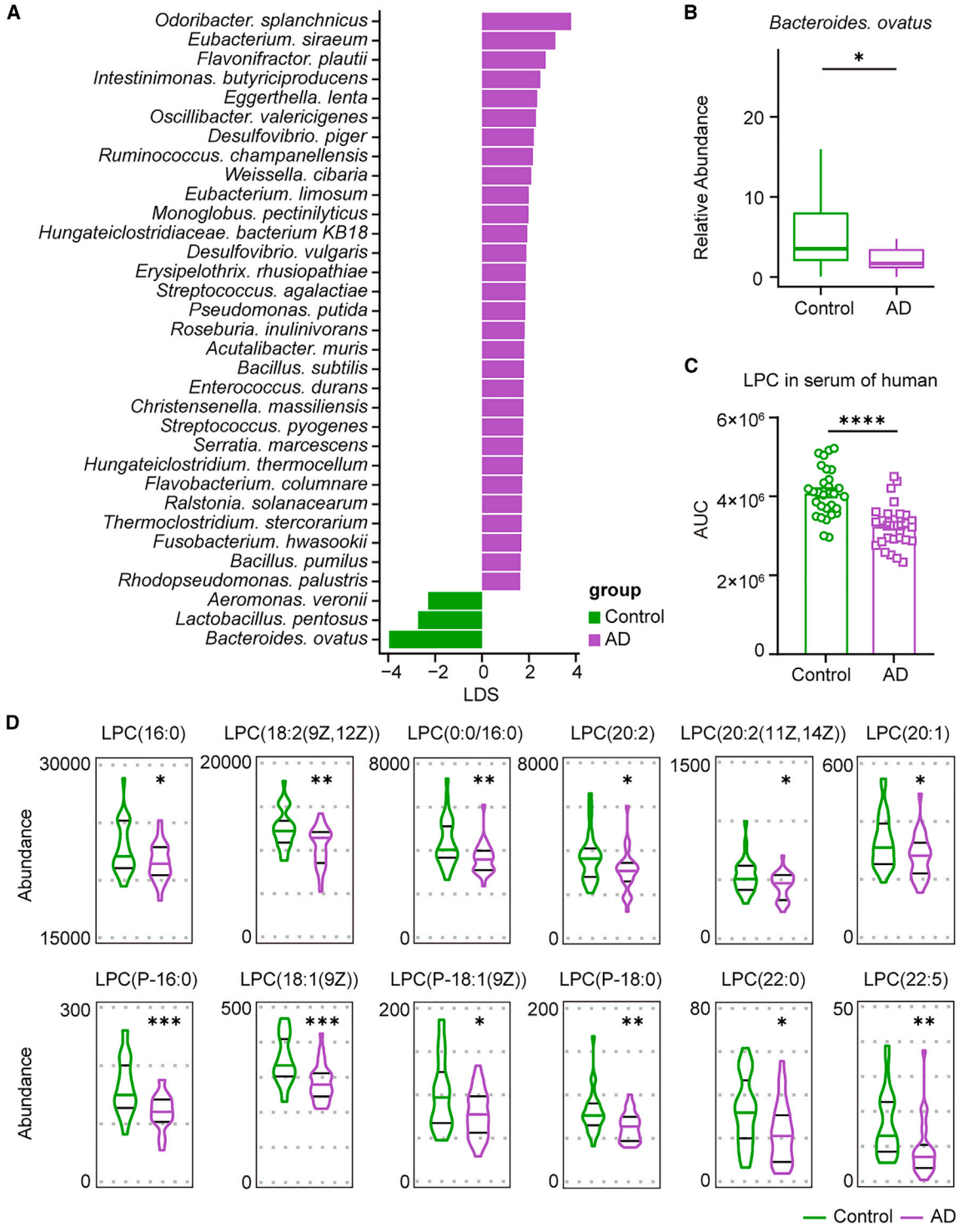

Figure 7. *B. ovatus* and LPC exhibit decreased levels in patients with AD

(A) LEfSe analysis of significant alterations in bacterial taxa at the species level.

(B) Bar plot showing the relative abundance of *B. ovatus* between control group and AD group.

(C) UPLC-MS analysis of LPC content in the serum of healthy individuals and patients with AD.

(D) Violin plot showing changes in the contents of LPC which significant decreased in the serum of AD subjects, as analyzed by lipidomics.

Data are presented as mean ± SEM. $^{*}p < 0.05$, $^{**}p < 0.01$, $^{***}p < 0.001$, $^{****}p < 0.0001$. (Wilcoxon Rank Sum and Signed Rank Tests in B. Unpaired t test in C and D).

See also Figure S7.

Please cite this article in press as: Zha et al., Microbiota-derived lysophosphatidylcholine alleviates Alzheimer's disease pathology via suppressing ferroptosis, Cell Metabolism (2024), https://doi.org/10.1016/j.cmet.2024.10.006

to a notable decrease in Aβ deposition in 5xFAD mice. Furthermore, recent research has established that the microbiota can significantly impact the progression of neurodegeneration in a tauopathy mouse model through increased p-tau pathology.[49] This underscores a causal role of the microbiota in the modulation of neurodegenerative processes. Our studies indicate that the gut microbiota of AD model mice is imbalanced; specifically, the abundance of *Clostridium* is increased, and the abundance of *Bacteroides* is reduced. Additionally, cohousing experiments demonstrated that outgrowth of *Clostridium* could directly lead to decreased colonization of *Bacteroides*. Our findings demonstrate that the loss of colonization and activity of *Bacteroides* in the intestinal tract of AD model mice and an increase in *Clostridium* abundance together lead to the progression of AD. The main mechanism by which *Clostridium* abundance increases in AD animal models is still unclear. Our study identified analogous alterations in *Bacteroides* within individuals with AD. While a moderate uptick in *Clostridium* abundance was also noted in AD, it did not reach statistical significance, aligning with previous findings.[51] This difference may be attributed to the fact that human and mouse microbiota share compositional similarities but exhibit significant quantitative discrepancies.[52] These observed variances between human and mouse studies are needed to deeper exploration and clarification in subsequent research.

Gut microbial symbionts form a key endocrine organ that converts nutrient factors in the environment into microbial-associated metabolites that play roles in normal physiology and disease in the human host.[53] LPC, a gut flora-regulated PC metabolite, is a critical regulator of normal brain growth and cognitive function by transporting docosahexaenoic acid (DHA) through orphan transporter Mfsd2a,[30] and PC and LPC are deficient in patients with AD.[31] Higher dietary PC intake was found to be associated with a lower risk of dementia in humans, albeit not in all studies.[32,54] Whether dietary intake of PC is related to cognitive decline and AD is still under debate. Our study found that in ABX-treated AD model mice, PC could not reduce Aβ deposition, suggesting that the effect of PC requires the gut microbiota. Our research also found that when PC is degraded into LPC by the gut microbiota, it can be transported to the brain, thereby exerting its effects, which suggests that LPC may be the active form of PC. Seo and colleagues found that short-chain fatty acids (SCFAs) produced by the gut microbiota could be involved in modulating tau-mediated neurodegeneration.[49] Similarly, our findings reveal that the relative abundance of many bacterial-family-level taxa associated with SCFAs production, such as Ruminococcaceae and Lachnospiraceae, were increased in the gut microbiota of AD model mice. Further characterization of the interaction between metabolites such as LPC and SCFAs, as well as the understanding of molecular mechanisms influencing Alzheimer's risk, may provide insights for future targeted therapies.

Our studies identified a mechanism of AD regulation that relies on the *Bacteroides*-LPC-GPR119-ferroptosis signaling axis. We demonstrate that the administration of LPC not only improves Aβ accumulation but also alleviates synaptic dysfunction, gliosis and myelin degeneration. These effects are achieved through the regulation of the ferroptosis signaling pathway. Our study revealed the presence of elevated lipid peroxidation levels and a significant increase in ROS production in the brains of mice model with AD. ROS induced lipid peroxidation is pivotal in cell death including apoptosis, autophagy, and ferroptosis.[55] Although apoptosis, pyroptosis, and autophagy were significantly increased in 5xFAD mice, our study preliminarily indicates that LPC may primarily exert its effects in AD mouse models through the modulation of ferroptosis. In addition, LPC supplementation regulated NRF2-ACSL4 axis through GPR119, resulting in the suppressing ferroptosis. However, our findings are not sufficient to support the conclusion that ferroptosis is the primary cause of Aβ deposition, and only suggest a potential mechanism concerning the beneficial effects of LPC on AD pathology. Future investigations should focus on examining whether and how ferroptosis impact on hallmarks of AD.

The GPR119 agonists have been verified to be safe for use *in vivo* and are being widely introduced into phase 2 clinical trials for the treatment of type 2 diabetes mellitus (T2DM).[56] We have found that GPR119 agonists can effectively alleviate AD symptoms. Through the research presented here, we indicate that interventions with the targets based on the *Bacteroides*-LPC-GPR119-ferroptosis axis show transformative potential for the treatment of AD.

Limitations of the study

Although our study founded microbiota and metabolites with neuromodulatory activity and defined the existence of a gut-microbiome-brain connection in AD model mice, several limitations should be discussed. First, our study indicated that *Clostridium* increase in abundance can directly affect the colonization of many *Bacteroides* species; however, how this occurs remains unknown, and subsequent research is required to elucidate the underlying mechanism. Second, our study although demonstrated clear role for *B. ovatus* and LPC in ameliorating AD pathology, other microbiota and metabolites may have similar effects, and studies will be needed to examine their roles and mechanisms in the future. Third, AD is characterized as a dual proteinopathy where the pathogenesis is propelled by the Aβ deposition and the aggregated tau accumulation.[57] While our study demonstrated clear role for *B. ovatus* and LPC in ameliorating Aβ deposition, further studies to characterize the roles and mechanisms of the *B. ovatus* and LPC to tau pathology are important. Finally, our research was mainly validated on mice, and the results may not be extended to humans at this stage. Additionally, the limited size of our human cohort represents another limitation. Future research will need to incorporate larger human cohorts to substantiate the present findings.

RESOURCE AVAILABILITY

Lead contact

Further information and requests for resources and reagents should be directed to and will be fulfilled by the lead contact, Dr. Chen Zhang (czhang@ccmu.edu.cn).

Materials availability

This study did not generate new unique reagents.

Data and code availability

- The raw metadata, raw single-cell RNA-seq data, and RNA-seq data are available online through the NGDC website (https://ngdc.cncb.ac.cn/)

with the study accession ID NGDC: PRJCA013503, PRJCA020474, PRJCA020467, OMIX002459, OMIX002669, and OMIX005085.
- This paper does not report the original code.
- Unprocessed data in this manuscript are available as Data S1-Source Data. Supplemental tables and figures are available as supplemental information.
- Any additional information required to reanalyze the data reported in this paper is available from the lead contact upon request.

ACKNOWLEDGMENTS

This work was supported by the National Natural Science Foundation of China (81925011, 92149304, 82073126, 32171120, 31871147, and 81874076), the Key-Area Research and Development Program of Guangdong Province (2019B030335001), the Youth Beijing Scholars Program (015), and the Joint Project of Municipal Education Commission and Municipal Foundation of Beijing (KZ202010025038). We extend our gratitude to the clinicians, researchers, and staff for their efforts in collecting and processing patient samples, including Yi Tang, Qiaoran Lin, and Xiaosheng Meng. All data are archived in Capital Medical University.

AUTHOR CONTRIBUTIONS

Conceptualization, C.Z., W.W., and X.L.; methodology, X.Z. and X.L.; formal analysis, H.H. and X.L.; investigation, X.Z., X.L., M.W., H.H., J.C., S.L., X.B., F.X., Y.Z., and Y.X.; writing – original draft, X.Z. and X.L.; writing – review & editing, X.Z., C.Z., W.W., and X.L.; funding acquisition, C.Z., W.W., and X.L.; resources, W.W. and C.Z.; supervision, C.Z., W.W., and X.L.

DECLARATION OF INTERESTS

The authors declare no competing interests.

STAR★METHODS

Detailed methods are provided in the online version of this paper and include the following:

- KEY RESOURCES TABLE
- EXPERIMENTAL MODEL AND SUBJECT DETAILS
  - Human subjects
  - Animal models
  - Germ-free mice and treatment
- METHOD DETAILS
  - ABX cocktail treatment
  - Sample collection and DNA extraction
  - Nanopore library preparation and sequencing
  - Metagenomics analysis
  - Bacterial strains culture and Microbial colonization
  - Quantitative PCR for microbiota analysis
  - Administration of drugs to SPF mice
  - Preparation of mouse tissue samples
  - Immunofluorescence
  - NOR test
  - MWM test
  - CFC test
  - Slice preparation and electrophysiological recordings
  - TEM
  - Untargeted metabolomics
  - UPLC-MS and Lipidomics
  - Metabolomic and metagenomic data correlation analysis
  - Single-cell sorting
  - Single-cell sequencing (Smart-seq2)
  - Smart-seq2 data processing
  - Quantitative reverse transcription PCR
  - Western blot assay
  - Malondialdehyde (MDA) content
  - Cell lines and culture conditions
  - Knockout and overexpression of target genes
  - Cell ferroptosis treatment and assessment
  - Flow cytometry
  - FMT experiments
  - Egg yolk agar plate assay for phospholipase activity
  - Expression of phospholipase A2 in *E. coli*
  - RNA-sequencing
- QUANTIFICATION AND STATISTICAL ANALYSIS

SUPPLEMENTAL INFORMATION

Supplemental information can be found online at https://doi.org/10.1016/j.cmet.2024.10.006.

Received: October 27, 2023
Revised: April 16, 2024
Accepted: October 4, 2024
Published: November 6, 2024

REFERENCES

1. Blennow, K., de Leon, M.J., and Zetterberg, H. (2006). Alzheimer's disease. Lancet *368*, 387–403. https://doi.org/10.1016/S0140-6736(06)69113-7.
2. Panza, F., Lozupone, M., Logroscino, G., and Imbimbo, B.P. (2019). A critical appraisal of amyloid-beta-targeting therapies for Alzheimer disease. Nat. Rev. Neurol. *15*, 73–88. https://doi.org/10.1038/s41582-018-0116-6.
3. Kametani, F., and Hasegawa, M. (2018). Reconsideration of Amyloid Hypothesis and Tau Hypothesis in Alzheimer's Disease. Front. Neurosci. *12*, 25. https://doi.org/10.3389/fnins.2018.00025.
4. Chen, X.Q., and Mobley, W.C. (2019). Exploring the Pathogenesis of Alzheimer Disease in Basal Forebrain Cholinergic Neurons: Converging Insights From Alternative Hypotheses. Front. Neurosci. *13*, 446. https://doi.org/10.3389/fnins.2019.00446.
5. Long, J.M., and Holtzman, D.M. (2019). Alzheimer Disease: An Update on Pathobiology and Treatment Strategies. Cell *179*, 312–339. https://doi.org/10.1016/j.cell.2019.09.001.
6. Jucker, M., and Walker, L.C. (2023). Alzheimer's disease: From immunotherapy to immunoprevention. Cell *186*, 4260–4270. https://doi.org/10.1016/j.cell.2023.08.021.
7. Holmes, C., Boche, D., Wilkinson, D., Yadegarfar, G., Hopkins, V., Bayer, A., Jones, R.W., Bullock, R., Love, S., Neal, J.W., et al. (2008). Long-term effects of Abeta42 immunisation in Alzheimer's disease: follow-up of a randomised, placebo-controlled phase I trial. Lancet *372*, 216–223. https://doi.org/10.1016/S0140-6736(08)61075-2.
8. Uhlmann, R.E., Rother, C., Rasmussen, J., Schelle, J., Bergmann, C., Ullrich Gavilanes, E.M., Fritschi, S.K., Buehler, A., Baumann, F., Skodras, A., et al. (2020). Acute targeting of pre-amyloid seeds in transgenic mice reduces Alzheimer-like pathology later in life. Nat. Neurosci. *23*, 1580–1588. https://doi.org/10.1038/s41593-020-00737-w.
9. Shabbir, U., Arshad, M.S., Sameen, A., and Oh, D.H. (2021). Crosstalk between Gut and Brain in Alzheimer's Disease: The Role of Gut Microbiota Modulation Strategies. Nutrients *13*, 690. https://doi.org/10.3390/nu13020690.
10. Bäuerl, C., Collado, M.C., Diaz Cuevas, A., Viña, J., and Pérez Martínez, G. (2018). Shifts in gut microbiota composition in an APP/PSS1 transgenic mouse model of Alzheimer's disease during lifespan. Lett. Appl. Microbiol. *66*, 464–471. https://doi.org/10.1111/lam.12882.
11. Zhan, X., Stamova, B., Jin, L.W., DeCarli, C., Phinney, B., and Sharp, F.R. (2016). Gram-negative bacterial molecules associate with Alzheimer disease pathology. Neurology *87*, 2324–2332. https://doi.org/10.1212/WNL.0000000000003391.
12. Vogt, N.M., Kerby, R.L., Dill-McFarland, K.A., Harding, S.J., Merluzzi, A.P., Johnson, S.C., Carlsson, C.M., Asthana, S., Zetterberg, H., Blennow, K., et al. (2017). Gut microbiome alterations in Alzheimer''s disease. Sci. Rep. *7*, 13537. https://doi.org/10.1038/s41598-017-13601-y.

13. Harach, T., Marungruang, N., Duthilleul, N., Cheatham, V., Mc Coy, K.D., Frisoni, G., Neher, J.J., Fåk, F., Jucker, M., Lasser, T., et al. (2017). Reduction of Abeta amyloid pathology in APPPS1 transgenic mice in the absence of gut microbiota. Sci. Rep. *7*, 41802. https://doi.org/10.1038/srep41802.

14. Minter, M.R., Zhang, C., Leone, V., Ringus, D.L., Zhang, X., Oyler-Castrillo, P., Musch, M.W., Liao, F., Ward, J.F., Holtzman, D.M., et al. (2016). Antibiotic-induced perturbations in gut microbial diversity influences neuro-inflammation and amyloidosis in a murine model of Alzheimer's disease. Sci. Rep. *6*, 30028. https://doi.org/10.1038/srep30028.

15. Wang, X., Sun, G., Feng, T., Zhang, J., Huang, X., Wang, T., Xie, Z., Chu, X., Yang, J., Wang, H., et al. (2019). Sodium oligomannate therapeutically remodels gut microbiota and suppresses gut bacterial amino acids-shaped neuroinflammation to inhibit Alzheimer's disease progression. Cell Res. *29*, 787–803. https://doi.org/10.1038/s41422-019-0216-x.

16. Erny, D., Hrabě de Angelis, A.L., Jaitin, D., Wieghofer, P., Staszewski, O., David, E., Keren-Shaul, H., Mahlakoiv, T., Jakobshagen, K., Buch, T., et al. (2015). Host microbiota constantly control maturation and function of microglia in the CNS. Nat. Neurosci. *18*, 965–977. https://doi.org/10.1038/nn.4030.

17. Needham, B.D., Funabashi, M., Adame, M.D., Wang, Z., Boktor, J.C., Haney, J., Wu, W.L., Rabut, C., Ladinsky, M.S., Hwang, S.J., et al. (2022). A gut-derived metabolite alters brain activity and anxiety behaviour in mice. Nature *602*, 647–653. https://doi.org/10.1038/s41586-022-04396-8.

18. Duan, Y., Ye, T., Qu, Z., Chen, Y., Miranda, A., Zhou, X., Lok, K.C., Chen, Y., Fu, A.K.Y., Gradinaru, V., et al. (2022). Brain-wide Cas9-mediated cleavage of a gene causing familial Alzheimer's disease alleviates amyloid-related pathologies in mice. Nat. Biomed. Eng. *6*, 168–180. https://doi.org/10.1038/s41551-021-00759-0.

19. Zhao, Y., and Lukiw, W.J. (2018). Bacteroidetes Neurotoxins and Inflammatory Neurodegeneration. Mol. Neurobiol. *55*, 9100–9107. https://doi.org/10.1007/s12035-018-1015-y.

20. Zhuang, Z.Q., Shen, L.L., Li, W.W., Fu, X., Zeng, F., Gui, L., Lü, Y., Cai, M., Zhu, C., Tan, Y.L., et al. (2018). Gut Microbiota is Altered in Patients with Alzheimer's Disease. J. Alzheimers Dis. *63*, 1337–1346. https://doi.org/10.3233/JAD-180176.

21. Shankar, G.M., Bloodgood, B.L., Townsend, M., Walsh, D.M., Selkoe, D.J., and Sabatini, B.L. (2007). Natural oligomers of the Alzheimer amyloid-beta protein induce reversible synapse loss by modulating an NMDA-type glutamate receptor-dependent signaling pathway. J. Neurosci. *27*, 2866–2875. https://doi.org/10.1523/JNEUROSCI.4970-06.2007.

22. Zhao, Y., Sivaji, S., Chiang, M.C., Ali, H., Zukowski, M., Ali, S., Kennedy, B., Sklyar, A., Cheng, A., Guo, Z., et al. (2017). Amyloid Beta Peptides Block New Synapse Assembly by Nogo Receptor-Mediated Inhibition of T-Type Calcium Channels. Neuron *96*, 355–372.e6. https://doi.org/10.1016/j.neuron.2017.09.041.

23. Gowrishankar, S., Yuan, P., Wu, Y., Schrag, M., Paradise, S., Grutzendler, J., De Camilli, P., and Ferguson, S.M. (2015). Massive accumulation of luminal protease-deficient axonal lysosomes at Alzheimer's disease amyloid plaques. Proc. Natl. Acad. Sci. USA *112*, E3699–E3708. https://doi.org/10.1073/pnas.1510329112.

24. Oakley, H., Cole, S.L., Logan, S., Maus, E., Shao, P., Craft, J., Guillozet-Bongaarts, A., Ohno, M., Disterhoft, J., Van Eldik, L., et al. (2006). Intraneuronal beta-amyloid aggregates, neurodegeneration, and neuron loss in transgenic mice with five familial Alzheimer's disease mutations: potential factors in amyloid plaque formation. J. Neurosci. *26*, 10129–10140. https://doi.org/10.1523/JNEUROSCI.1202-06.2006.

25. Wilson, D.M., 3rd, Cookson, M.R., Van Den Bosch, L., Zetterberg, H., Holtzman, D.M., and Dewachter, I. (2023). Hallmarks of neurodegenerative diseases. Cell *186*, 693–714. https://doi.org/10.1016/j.cell.2022.12.032.

26. Zhang, X., Wang, R., Hu, D., Sun, X., Fujioka, H., Lundberg, K., Chan, E.R., Wang, Q., Xu, R., Flanagan, M.E., et al. (2020). Oligodendroglial glycolytic stress triggers inflammasome activation and neuropathology in Alzheimer's disease. Sci. Adv. *6*, eabb8680. https://doi.org/10.1126/sciadv.abb8680.

27. Depp, C., Sun, T., Sasmita, A.O., Spieth, L., Berghoff, S.A., Nazarenko, T., Overhoff, K., Steixner-Kumar, A.A., Subramanian, S., Arinrad, S., et al. (2023). Myelin dysfunction drives amyloid-beta deposition in models of Alzheimer's disease. Nature *618*, 349–357. https://doi.org/10.1038/s41586-023-06120-6.

28. Buffington, S.A., Dooling, S.W., Sgritta, M., Noecker, C., Murillo, O.D., Felice, D.F., Turnbaugh, P.J., and Costa-Mattioli, M. (2021). Dissecting the contribution of host genetics and the microbiome in complex behaviors. Cell *184*, 1740–1756.e16. https://doi.org/10.1016/j.cell.2021.02.009.

29. Walter, A., Korth, U., Hilgert, M., Hartmann, J., Weichel, O., Hilgert, M., Fassbender, K., Schmitt, A., and Klein, J. (2004). Glycerophosphocholine is elevated in cerebrospinal fluid of Alzheimer patients. Neurobiol. Aging *25*, 1299–1303. https://doi.org/10.1016/j.neurobiolaging.2004.02.016.

30. Nguyen, L.N., Ma, D., Shui, G., Wong, P., Cazenave-Gassiot, A., Zhang, X., Wenk, M.R., Goh, E.L.K., and Silver, D.L. (2014). Mfsd2a is a transporter for the essential omega-3 fatty acid docosahexaenoic acid. Nature *509*, 503–506. https://doi.org/10.1038/nature13241.

31. Mapstone, M., Cheema, A.K., Fiandaca, M.S., Zhong, X., Mhyre, T.R., MacArthur, L.H., Hall, W.J., Fisher, S.G., Peterson, D.R., Haley, J.M., et al. (2014). Plasma phospholipids identify antecedent memory impairment in older adults. Nat. Med. *20*, 415–418. https://doi.org/10.1038/nm.3466.

32. Ylilauri, M.P.T., Voutilainen, S., Lönnroos, E., Virtanen, H.E.K., Tuomainen, T.P., Salonen, J.T., and Virtanen, J.K. (2019). Associations of dietary choline intake with risk of incident dementia and with cognitive performance: the Kuopio Ischaemic Heart Disease Risk Factor Study. Am. J. Clin. Nutr. *110*, 1416–1423. https://doi.org/10.1093/ajcn/nqz148.

33. Aparicio Vizuete, A., Robles, F., Rodríguez-Rodríguez, E., López-Sobaler, A.M., and Ortega, R.M. (2010). Association between food and nutrient intakes and cognitive capacity in a group of institutionalized elderly people. Eur. J. Nutr. *49*, 293–300. https://doi.org/10.1007/s00394-009-0086-y.

34. Qiu, B., Zandkarimi, F., Bezjian, C.T., Reznik, E., Soni, R.K., Gu, W., Jiang, X., and Stockwell, B.R. (2024). Phospholipids with two polyunsaturated fatty acyl tails promote ferroptosis. Cell *187*, 1177–1190.e18. https://doi.org/10.1016/j.cell.2024.01.030.

35. Stockwell, B.R. (2022). Ferroptosis turns 10: Emerging mechanisms, physiological functions, and therapeutic applications. Cell *185*, 2401–2421. https://doi.org/10.1016/j.cell.2022.06.003.

36. Xie, Y., Hou, W., Song, X., Yu, Y., Huang, J., Sun, X., Kang, R., and Tang, D. (2016). Ferroptosis: process and function. Cell Death Differ. *23*, 369–379. https://doi.org/10.1038/cdd.2015.158.

37. Doll, S., Proneth, B., Tyurina, Y.Y., Panzilius, E., Kobayashi, S., Ingold, I., Irmler, M., Beckers, J., Aichler, M., Walch, A., et al. (2017). ACSL4 dictates ferroptosis sensitivity by shaping cellular lipid composition. Nat. Chem. Biol. *13*, 91–98. https://doi.org/10.1038/nchembio.2239.

38. Liang, D., Feng, Y., Zandkarimi, F., Wang, H., Zhang, Z., Kim, J., Cai, Y., Gu, W., Stockwell, B.R., and Jiang, X. (2023). Ferroptosis surveillance independent of GPX4 and differentially regulated by sex hormones. Cell *186*, 2748–2764.e22. https://doi.org/10.1016/j.cell.2023.05.003.

39. Chen, X., Li, J., Kang, R., Klionsky, D.J., and Tang, D. (2021). Ferroptosis: machinery and regulation. Autophagy *17*, 2054–2081. https://doi.org/10.1080/15548627.2020.1810918.

40. Kim, R., Hashimoto, A., Markosyan, N., Tyurin, V.A., Tyurina, Y.Y., Kar, G., Fu, S., Sehgal, M., Garcia-Gerique, L., Kossenkov, A., et al. (2022). Ferroptosis of tumour neutrophils causes immune suppression in cancer. Nature *612*, 338–346. https://doi.org/10.1038/s41586-022-05443-0.

41. Doll, S., Freitas, F.P., Shah, R., Aldrovandi, M., da Silva, M.C., Ingold, I., Goya Grocin, A., Xavier da Silva, T.N., Panzilius, E., Scheel, C.H., et al. (2019). FSP1 is a glutathione-independent ferroptosis suppressor. Nature *575*, 693–698. https://doi.org/10.1038/s41586-019-1707-0.

42. Xu, P., Huang, S., Guo, S., Yun, Y., Cheng, X., He, X., Cai, P., Lan, Y., Zhou, H., Jiang, H., et al. (2022). Structural identification of lysophosphatidylcholines as activating ligands for orphan receptor GPR119. Nat. Struct. Mol. Biol. *29*, 863–870. https://doi.org/10.1038/s41594-022-00816-5.

43. Song, X., and Long, D. (2020). Nrf2 and Ferroptosis: A New Research Direction for Neurodegenerative Diseases. Front. Neurosci. *14*, 267. https://doi.org/10.3389/fnins.2020.00267.

44. Wang, J., Zhu, Q., Wang, Y., Peng, J., Shao, L., and Li, X. (2022). Irisin protects against sepsis-associated encephalopathy by suppressing ferroptosis via activation of the Nrf2/GPX4 signal axis. Free Radic. Biol. Med. *187*, 171–184. https://doi.org/10.1016/j.freeradbiomed.2022.05.023.

45. Matheoud, D., Cannon, T., Voisin, A., Penttinen, A.M., Ramet, L., Fahmy, A.M., Ducrot, C., Laplante, A., Bourque, M.J., Zhu, L., et al. (2019). Intestinal infection triggers Parkinson's disease-like symptoms in Pink1$^{-/-}$ mice. Nature *571*, 565–569. https://doi.org/10.1038/s41586-019-1405-y.

46. Sampson, T.R., Debelius, J.W., Thron, T., Janssen, S., Shastri, G.G., Ilhan, Z.E., Challis, C., Schretter, C.E., Rocha, S., Gradinaru, V., et al. (2016). Gut Microbiota Regulate Motor Deficits and Neuroinflammation in a Model of Parkinson's Disease. Cell *167*, 1469–1480.e12. https://doi.org/10.1016/j.cell.2016.11.018.

47. Burberry, A., Wells, M.F., Limone, F., Couto, A., Smith, K.S., Keaney, J., Gillet, G., van Gastel, N., Wang, J.Y., Pietilainen, O., et al. (2020). C9orf72 suppresses systemic and neural inflammation induced by gut bacteria. Nature *582*, 89–94. https://doi.org/10.1038/s41586-020-2288-7.

48. Bosch, M.E., Dodiya, H.B., Michalkiewicz, J., Lee, C., Shaik, S.M., Weigle, I.Q., Zhang, C., Osborn, J., Nambiar, A., Patel, P., et al. (2024). Sodium oligomannate alters gut microbiota, reduces cerebral amyloidosis and reactive microglia in a sex-specific manner. Mol. Neurodegener. *19*, 18. https://doi.org/10.1186/s13024-023-00700-w.

49. Seo, D.O., O'Donnell, D., Jain, N., Ulrich, J.D., Herz, J., Li, Y., Lemieux, M., Cheng, J., Hu, H., Serrano, J.R., et al. (2023). ApoE isoform- and microbiota-dependent progression of neurodegeneration in a mouse model of tauopathy. Science *379*, eadd1236. https://doi.org/10.1126/science.add1236.

50. Chevalier, G., Siopi, E., Guenin-Macé, L., Pascal, M., Laval, T., Rifflet, A., Boneca, I.G., Demangel, C., Colsch, B., Pruvost, A., et al. (2020). Effect of gut microbiota on depressive-like behaviors in mice is mediated by the endocannabinoid system. Nat. Commun. *11*, 6363. https://doi.org/10.1038/s41467-020-19931-2.

51. Ferreiro, A.L., Choi, J., Ryou, J., Newcomer, E.P., Thompson, R., Bollinger, R.M., Hall-Moore, C., Ndao, I.M., Sax, L., Benzinger, T.L.S., et al. (2023). Gut microbiome composition may be an indicator of preclinical Alzheimer's disease. Sci. Transl. Med. *15*, eabo2984. https://doi.org/10.1126/scitranslmed.abo2984.

52. Hugenholtz, F., and de Vos, W.M. (2018). Mouse models for human intestinal microbiota research: a critical evaluation. Cell. Mol. Life Sci. *75*, 149–160. https://doi.org/10.1007/s00018-017-2693-8.

53. Wang, Z., Roberts, A.B., Buffa, J.A., Levison, B.S., Zhu, W., Org, E., Gu, X., Huang, Y., Zamanian-Daryoush, M., Culley, M.K., et al. (2015). Non-lethal Inhibition of Gut Microbial Trimethylamine Production for the Treatment of Atherosclerosis. Cell *163*, 1585–1595. https://doi.org/10.1016/j.cell.2015.11.055.

54. Iannotti, L.L., Lutter, C.K., Waters, W.F., Gallegos Riofrío, C.A., Malo, C., Reinhart, G., Palacios, A., Karp, C., Chapnick, M., Cox, K., et al. (2017). Eggs early in complementary feeding increase choline pathway biomarkers and DHA: a randomized controlled trial in Ecuador. Am. J. Clin. Nutr. *106*, 1482–1489. https://doi.org/10.3945/ajcn.117.160515.

55. Su, L.J., Zhang, J.H., Gomez, H., Murugan, R., Hong, X., Xu, D., Jiang, F., and Peng, Z.Y. (2019). Reactive Oxygen Species-Induced Lipid Peroxidation in Apoptosis, Autophagy, and Ferroptosis. Oxid. Med. Cell. Longev. *2019*, 5080843. https://doi.org/10.1155/2019/5080843.

56. Manaithiya, A., Alam, O., Sharma, V., Javed Naim, M., Mittal, S., and Khan, I.A. (2021). GPR119 agonists: novel therapeutic agents for type 2 diabetes mellitus. Bioorg. Chem. *113*, 104998. https://doi.org/10.1016/j.bioorg.2021.104998.

57. Gallardo, G., and Holtzman, D.M. (2019). Amyloid-beta and Tau at the Crossroads of Alzheimer's Disease. Adv. Exp. Med. Biol. *1184*, 187–203. https://doi.org/10.1007/978-981-32-9358-8_16.

58. Vaishnava, S., Yamamoto, M., Severson, K. M., Ruhn, K. A., Yu, X., Koren, O., Ley, R., Wakeland, E. K., and Hooper, L.V. (2011). The antibacterial lectin RegIIIgamma promotes the spatial segregation of microbiota and host in the intestine. Science *334*, 255–258.

59. Seiler, A., Schneider, M., Förster, H., Roth, S., Wirth, E.K., Culmsee, C., Plesnila, N., Kremmer, E., Rådmark, O., Wurst, W., et al. (2008). Glutathione peroxidase 4 senses and translates oxidative stress into 12/15-lipoxygenase dependent- and AIF-mediated cell death. Cell Metab. *8*, 237–248. https://doi.org/10.1016/j.cmet.2008.07.005.

60. Bevins, R.A., and Besheer, J. (2006). Object recognition in rats and mice: a one-trial non-matching-to-sample learning task to study 'recognition memory'. Nat. Protoc. *1*, 1306–1311. https://doi.org/10.1038/nprot.2006.205.

61. Vorhees, C.V., and Williams, M.T. (2006). Morris water maze: procedures for assessing spatial and related forms of learning and memory. Nat. Protoc. *1*, 848–858. https://doi.org/10.1038/nprot.2006.116.

62. Shen, L., Feng, C., Zhang, K., Chen, Y., Gao, Y., Ke, J., Chen, X., Lin, J., Li, C., Iqbal, J., et al. (2019). Proteomics Study of Peripheral Blood Mononuclear Cells (PBMCs) in Autistic Children. Front. Cell. Neurosci. *13*, 105. https://doi.org/10.3389/fncel.2019.00105.

63. Wei, M., Zhang, J., Jia, M., Yang, C., Pan, Y., Li, S., Luo, Y., Zheng, J., Ji, J., Chen, J., et al. (2016). α/β-Hydrolase domain-containing 6 (ABHD6) negatively regulates the surface delivery and synaptic function of AMPA receptors. Proc. Natl. Acad. Sci. USA *113*, E2695–E2704. https://doi.org/10.1073/pnas.1524589113.

Please cite this article in press as: Zha et al., Microbiota-derived lysophosphatidylcholine alleviates Alzheimer's disease pathology via suppressing ferroptosis, Cell Metabolism (2024), https://doi.org/10.1016/j.cmet.2024.10.006

STAR★METHODS

KEY RESOURCES TABLE

REAGENT or RESOURCE	SOURCE	IDENTIFIER
Antibodies		
Mouse monoclonal anti-6E10	Biolegend	Cat # 803014; RRID: AB_2728527
Rabbit polyclonal anti-Aβ	Cell Signaling Technology	Cat # 2425S
Rabbit polyclonal anti-Iba1	Wako	Cat # 019-19741; RRID: AB_839504
Rabbit polyclonal anti-GFAP	Abcam	Cat # ab7260; RRID: AB_305808
Rabbit polyclonal anti-LAMP1	Abcam	Cat # ab24170; RRID: AB_775978
Alexa Fluor 488 Polyclonal Antibody	Invitrogen	Cat # A11094; RRID: AB_221544
Alexa Fluor 594 Polyclonal Antibody	Invitrogen	Cat # A11005; RRID: AB_2534073
Rabbit monoclonal anti-GPX4	Abcam	Cat # ab125066; RRID: AB_10973901
Rabbit monoclonal anti-FACL4	Abcam	Cat # ab155282; RRID: AB_2714020
Rabbit polyclonal anti-NRF2	Invitrogen	Cat # PA5-27882; RRID: AB_2545358
Mouse monoclonal anti-FSP1	Santa Cruz Biotechnology	Cat # sc-377120; RRID: AB_2893240
Rabbit polyclonal anti-MBOAT1	Affinit Bioscience	Cat # DF15819
Rabbit monoclonal anti-GSDMD	Abcam	Cat # ab219800; RRID: AB_2888940
Rabbit monoclonal anti- LC3B	Abcam	ab192890; RRID: AB_2827794
Mouse monoclonal anti-actin	Cell Signaling Technology	Cat # 3700; RRID: AB_2242334
Bacterial and virus strains		
Bacteroides ovatus	ATCC	Cat # BAA-1304
Bacteroides caccae	ATCC	Cat # 43185
Bacteroides vulgatus	JCM	Cat # 5826T
Bacteroides dorei	JCM	Cat # 13471T
Bacteroides thetaiotaomicron	JCM	Cat # 5827T
Clostridium beijerinckii	ATCC	Cat # 17778
Clostridium acetobutylicum	CGMCC	Cat # 1.5074
Clostridium sporogenes	CGMCC	Cat # 1.5212
Escherichia coli BL21 (DE3)	TransGen Biotech	Cat # CD601-02
Biological samples		
Human feces and serum samples	Xuanwu Hospital of Capital Medical University	N/A
Chemicals, peptides, and recombinant proteins		
Ampicillin sodium salt	Solarbio	Cat # A8180
Neomycin sulfate	Solarbio	Cat # A8090
Metronidazole	Solarbio	Cat # M8060
Vancomyci hydrochloride	MP Biomedicals	Cat # 02195540
NEBNext Ultra II End Repair/dA-Tailing Module	New England Biolabs	Cat # E7546
NEBNext FFPE DNA Repair Mix	New England Biolabs	Cat # M6630
NEB Quick Ligation Module	New England Biolabs	Cat # E6056
NEBNext Blunt/TA Ligase Master Mix	New England Biolabs	Cat # M0367
EG broth medium	Hopebio	Cat # HB8594
PYG broth medium	Hopebio	Cat # HB0398
10% egg yolk salt solution	Hopebio	Cat # HB5221a
TRIzol	Life Technologies	Cat # 15596026
Tribromoethanol	Sigma	Cat # T48402
10X Dulbecco's Phosphate-Buffered Saline (PBS)	Sigma	Cat # D1408
PC	Sigma	Cat # P3556

(*Continued on next page*)

Please cite this article in press as: Zha et al., Microbiota-derived lysophosphatidylcholine alleviates Alzheimer's disease pathology via suppressing ferroptosis, Cell Metabolism (2024), https://doi.org/10.1016/j.cmet.2024.10.006

Continued

REAGENT or RESOURCE	SOURCE	IDENTIFIER
LPC	Sigma	Cat # L4129
EcoRI-HF	New England Biolabs	Cat # R3101S
T4 DNA Ligase	New England Biolabs	Cat # M0202S
Isopropyl-β-D-thiogalactopyranoside (IPTG)	MedChemExpress	Cat # HY-15921
RSL3	MedChemExpress	Cat # HY-100218A
Erastin	Abmole	Cat # M2679
Liproxstatin-1	Sigma	Cat # SML1414
Paraformaldehyde (PFA)	Sigma	Cat # P6148
Glutaraldehyde	Sigma	Cat # G5882
Triton X-100	Amresco	Cat # 9,002,931
Bovine serum albumin	Sigma	Cat # A1933
4',6-diamidino-2-phenylindole (DAPI)	Beyotime	Cat # C1006
Ammonium acetate	Supelco	Cat # 73594
Methanol	Innochem	Cat # M6600
Acetonitrile	Sigma	Cat # 34851
Isopropanol	Sigma	Cat # 34863
RIPA lysis buffer	Applygen Technology	Cat # C1053
PMSF	Beyotime Biotechnology	Cat # ST506
DMEM	GIBCO-Invitrogen	Cat # 11960044
FBS	GIBCO-Invitrogen	Cat # 16140071
C11-BODIPY	ThermoFisher Scientific	Cat # D3861
SPY-LHP	Dojindo	Cat # L248
Penicillin/streptomycin	GIBCO-Invitrogen	Cat # 15140122
APD668	MedChemExpress	Cat # HY-15565
Complete Protease Inhibitor EASY Packs EDTA-Free	Roche	Cat # 04693132001
CellROX™ Green	Invitrogen	Cat # C10444
Zombie Yellow solution	BioLegend	Cat # 423104
Cell Staining Buffer	BioLegend	Cat # 420201
AMPure XP beads	Beckman	Cat# A63881
MinION flow cells (R9.4.1)	Oxford Nanopore Technologies	Cat# FLO-MIN106D
OCT compound	Sakura	Cat# 4583
Anti-O4 MicroBeads	Miltenyi Biotec	Cat# 130-094-543
Anti-CD11b (microglia) MicroBeads	Miltenyi Biotec	Cat# 130-093-634
Anti-ACSA-2 MicroBeads	Miltenyi Biotec	Cat# 130-095-825
Choline deficient (CD) diet	MP Biomedicals	Cat# 02960034-CF
PVDF membrane	Millipore	Cat # IPVH00010
Critical commercial assays		
FastDNA Spin Kit for Feces	MP Biomedicals	Cat# 116570200
Qubit 1X dsDNA HS Assay Kit	ThermoFisher Scientific	Cat# Q33230
Ligation Sequencing Kit	Oxford Nanopore Technologies	Cat# SQK-LSK109
Adult Brain Dissociation Kit	Miltenyi Biotec	Cat# 130-107-677
Adult Neuron Isolation Kit	Miltenyi Biotec	Cat# 130-042-303
ReadyProbes Cell Viability Imaging Kit	ThermoFisher Scientific	Cat# R37610
Agilent High Sensitivity DNA Kit	Agilent Technologies	Cat# 5067-4626
KAPA Library Quantification Kit	Kapa Biosystems	Cat# KK4824
FastPure Cell/Tissue Total RNA Isolation Kit	Vazyme Biotech	Cat# RC101-01
HiScript II One Step RT-PCR Kit	Vazyme Biotech	Cat# P612-01
PowerUp SYBR Green Master Mix	ThermoFisher Scientific	Cat# A25742

(*Continued on next page*)

Continued

REAGENT or RESOURCE	SOURCE	IDENTIFIER
Lipid Peroxidation (MDA) Assay Kit	Sigma	Cat# MAK085
Pierce BCA Protein Assay Kit	ThermoFisher Scientific	Cat # 23225
TUNEL BrightGreen Apoptosis Detection Kit	Vazyme Biotech	Cat # A112-01
alamarBlue™ HS Cell Viability Reagent	Invitrogen	Cat # A50100
LDH assay kit	Abcam	Cat # ab65393
Deposited data		
Database: Nanopore-based metagenomic sequencing analysis of 5xFAD mice (https://ngdc.cncb.ac.cn/bioproject/)	This study	Accession ID: PRJCA013503
Database: RNA sequencing of BV2 cells induced by ferroptosis (https://ngdc.cncb.ac.cn/bioproject/)	This study	Accession ID: PRJCA020474
Database: Nanopore-based metagenomic sequencing analysis of control subjects and patients with AD (https://ngdc.cncb.ac.cn/bioproject/)	This study	Accession ID: PRJCA020467
Database: Unbiased serum metabolomic profiling of 5xFAD mice (https://ngdc.cncb.ac.cn/omix/select-edit/OMIX002459)	This study	OMIX ID: OMIX002459
Database: Smart seq2 full-length RNA-sequencing of 5xFAD mice (https://ngdc.cncb.ac.cn/omix/select-edit/OMIX002669)	This study	OMIX ID: OMIX002669
Database: Lipidomics analysis of serum metabolomic profiling of control subjects and AD patients (https://ngdc.cncb.ac.cn/omix/select-edit/OMIX005085)	This study	OMIX ID: OMIX005085
Experimental models: Cell lines		
SH-SY5Y	ATCC	CRL-2266; RRID:CVCL_0019
BV2	BMCR	4201MOU-CCTCC00311; RRID:CVCL_0182
HT22	Ubigene	YC-A004; RRID:CVCL_0321
Experimental models: Organisms/strains		
Mouse: 5xFAD	The Jackson Laboratory	Cat# 034840
Mouse: 5xFAD	The Jackson Laboratory	Cat# 008730
Mouse: *Gpx4*$^{fl/fl}$	The Jackson Laboratory	Cat# 027964
Mouse: Nestin-Cre	The Jackson Laboratory	Cat# J003771
Mouse: *Acsl4*$^{fl/fl}$	Cyagen Biosciences	Cat# S-CKO-11400
Mouse: C57BL/6	Charles River	Cat# 219
Mouse: SJL	Charles River	Cat# 216
Oligonucleotides		
Eubacteria F 5-ACTCCTACGGGAGGCAGCAGT-3'	Vaishnava et al.[58]	N/A
Eubacteria R 5-ATTACCGCGGCTGCTGGC-3'	Vaishnava et al.[58]	N/A
Bacteroides F 5-GGTTCTGAGAGGAGGTCCC-3'	Vaishnava et al.[58]	N/A
Bacteroides R 5-CTGCCTCCCGTAGGAGT-3'	Vaishnava et al.[58]	N/A
Clostridium F 5-ACTCCTACGGGAGGCAGC-3'	Vaishnava et al.[58]	N/A
Clostridium R 5-GCTTCTTAGTCAGGTACCGTCA-3'	Vaishnava et al.[58]	N/A
ACSL4 F 5-CCTCCGATTGAAATCACAGAAGA-3'	This Study	N/A
ACSL4 R 5-GCCATAGCGTTTTTCTTAAATGTCC -3'	This Study	N/A
Actin F 5- CTTCGCGGGCGACGAT-3'	This Study	N/A
Actin R 5- CCACATAGGAATCCTTCTGACC-3'	This Study	N/A
Nrf2 F AGGTTGCCCACATTCCCAAA	This Study	N/A
Nrf2 R AGTGACTGAAACGTAGCCGA	This Study	N/A
gRNA (GPR119) CTGCACAGGGTCTTCTGTGT GGG	Ubigene	N/A
gRNA (ACSL4) AAGTGTGTGACAGAGCGATA TGG	Ubigene	N/A
gRNA (NFE2L2) TATTTGACTTCAGTCAGCGA CGG	Ubigene	N/A

(*Continued on next page*)

Please cite this article in press as: Zha et al., Microbiota-derived lysophosphatidylcholine alleviates Alzheimer's disease pathology via suppressing ferroptosis, Cell Metabolism (2024), https://doi.org/10.1016/j.cmet.2024.10.006

Continued

REAGENT or RESOURCE	SOURCE	IDENTIFIER
Software and algorithms		
Guppy V6.3.8	Oxford Nanopore Technologies	https://nanoporetech.com
R Studio	R Studio	https://rstudio.com
R	The R Foundation	https://www.r-project.org/foundation/index.html
ImageJ software	NIH	https://imagej.nih.gov/ij/
UNIFI 1.9.3 software	Waters MS Technologies	https://www.waters.com/nextgen/cn/zh/search.html?keyword=UNIFI%201.9.3%20software&sort=most-relevant
FlowJo software	Tree Star	https://www.flowjo.com/solutions/flowjo/downloads
GraphPad Prism 8.0	Graphpad Software	www.graphpad.com
Other		
AMPure XP beads	Beckman	Cat# A63881
MinION flow cells (R9.4.1)	Oxford Nanopore Technologies	Cat# FLO-MIN106D
OCT compound	Sakura	Cat# 4583
Anti-O4 MicroBeads	Miltenyi Biotec	Cat# 130-094-543
Anti-CD11b (microglia) MicroBeads	Miltenyi Biotec	Cat# 130-093-634
Anti-ACSA-2 MicroBeads	Miltenyi Biotec	Cat# 130-095-825
Choline deficient (CD) diet	MP Biomedicals	Cat# 02960034-CF
PVDF membrane	Millipore	Cat # IPVH00010

EXPERIMENTAL MODEL AND SUBJECT DETAILS

Human subjects

Patients diagnosed with AD and age-matched normal controls were recruited from Department of Neurology in Xuanwu Hospital of Capital Medical University. Patients with AD were diagnosed using the NINDS/ADRDA criteria and confirmed by experienced neurologists at Department of Neurology. The cognitive functions were evaluated using the Mini-Mental State Examination (MMSE) and the instrumental Montreal Cognitive Assessment (MoCA). In addition to questionnaires, all participants were screened according to their medical history, laboratory tests, physical and neurological examinations. Serum and fecal samples were collected from twenty-nine patients and twenty-nine age-matched normal controls. Subjects or next of kin provided informed consent and consented to the serum or feces donation. The study was approved by the Capital Medical University Institutional Review Board (Z2022SY091). Subject baseline characteristics of individuals with AD and controls are presented in Table S1.

Animal models

5xFAD, 3xTg-AD, *Gpx4*$^{fl/fl}$ and Nestin-Cre mice were bought from Jackson Laboratory. *Acsl4*$^{fl/fl}$ mice were procured from Cyagen Biosciences. C57BL/6 and SJL were purchased from Charles River. Mice were bred at Capital Medical University. Homozygous nervous system specific *Gpx4* knockout mice were neonatally lethal,[59] so we generated nervous system-specific *Gpx4* conditional knockout (CKO) hemizygous mice with the 5xFAD genetic background. All mice were kept under SPF conditions and provided with unrestricted access of water and food. For the choline-deficient model, mice at eight weeks of age were randomized to receive either a choline deficient (CD) diet or control chow diet ad libitum for 6 weeks. All experiments were conducted using male mice. the Animal Experimentation Committee of Capital Medical University set ethical standards for our procedures and treatments (797C083C-1A26-4599-AFC3-18E41F111E0A).

Germ-free mice and treatment

The male GF mice were individually housed in the sterile cages. In order to recolonize of GF mice with 5xFAD mice microbiota. Donor samples were collected from either WT or 5xFAD mice. A fecal suspension of 200 μL was administered to the recipient GF mice via oral gavage for a total of six times. Additionally, mice in their respective groups were administered *B. ovatus* via oral gavage or LPC via intraperitoneal injection.

Please cite this article in press as: Zha et al., Microbiota-derived lysophosphatidylcholine alleviates Alzheimer's disease pathology via suppressing ferroptosis, Cell Metabolism (2024), https://doi.org/10.1016/j.cmet.2024.10.006

METHOD DETAILS

ABX cocktail treatment

Mice were orally administered a mixture of ABX consisting of ampicillin sodium salt (0.5 mg/mL), neomycin sulfate (0.5 mg/mL), metronidazole (0.5 mg/mL) and vancomycin hydrochloride (0.25 mg/mL) via sterile drinking water. The timeframe of treatment slightly differed among mice of different ages. In the ABX treatment experiment, mice were administered ABX via drinking water continuously for one month from the age of 1 month. For 6-weeks-old, 4 and 10-month-old mice, antibiotics were administered beginning 2 weeks prior to subsequent administration via drinking water. The solutions were replaced twice per week. Twenty-two-day-old mice were administered ABX by oral gavage for 3 days using animal feeding syringes before undergoing bacterium treatment.

Sample collection and DNA extraction

Feces were collected in sterile EP tubes and freezed in liquid nitrogen rapidly then stored at −80°C. FastDNA Spin Kit for Feces were used to extract microbial DNA. The degradation and contamination of DNA were assessed with 1% agarose gels. DNA purity was evaluated by a Nanodrop spectrophotometer (ThermoFisher Scientific). DNA concentration was detected on a Qubit 4.0 Fluorometer (ThermoFisher Scientific).

Nanopore library preparation and sequencing

We used the Ligation Sequencing Kit (Oxford Nanopore Technologies) to make multiplexed nanopore sequencing libraries as directed by the manufacturer. In brief, 1000 ng of DNA per sample from 5xFAD and age-matched wild type mice were end-repaired using NEBNext Ultra II End Repair/dA-Tailing Module. NEBNext FFPE DNA Repair Mix, and AMPure XP beads were used to purify DNA. Next, Each DNA was ligated with a unique barcode with NEB Quick Ligation Module. After the concentration was measured with Qubit Fluorometer, twelve or more barcoded DNA samples were pooled in equal mass ratios. Then, the pooled barcoded samples were ligated to a sequencing adaptor for nanopore sequencing using NEBNext Blunt/TA Ligase Master Mix. Using a MinION flow cells to prime and load the ligation library, Subsequently, the Mk1C device is operated continuously for approximately 48-72 hours until no more reads can be obtained.

Metagenomics analysis

Using Guppy (v 6.3.8, Oxford Nanopore Technologies) to perform base calling offline on the raw reads obtained from fast5 files. Then the quality and read length were evaluate by minion_qc (v 1.4.2) and NanoPlot (v 1.33.0). The Shannon index was used to assess alpha diversity, while the Bray-Curtis index distance method (including PCoA and NMDS) were utilized to determine beta diversity. For beta diversity, Statistics were calculated using pairwise PERMANOVA. In order to visualize bacterial taxa that exhibited significant differences in abundance among samples from different groups, the Linear discriminant analysis effect size (LEfSe) was used. Statistical analyses of box plot were performed using Wilcoxon Rank Sum and Signed Rank Test.

Bacterial strains culture and Microbial colonization

B. ovatus, *B. vulgatus*, *B. dorei*, *B. caccae* and *B. thetaiotaomicron* were cultured in EG broth medium supplemented with 5% FBS under anaerobic conditions at 37°C. *C. beijerinckii*, *C. acetobutylicum* and *C.sporogenes* were grown in PYG broth medium at a temperature of 37°C within an anaerobic chamber, until the culture reached OD=0.8-1. ABX treated mice were colonized with 200 μl indicated bacteria consortia or the same volume of medium by oral gavage three times per week for 4 or 6 weeks.

Quantitative PCR for microbiota analysis

After microbiota colonization, feces of mice were collected and the gDNA were extracted. Then the concentrations of gDNA were quantified to 1ng/μL. The abundance of specific intestinal bacterial groups was quantified by PowerUp SYBR Green Master Mix using group-specific 16S rRNA gene primers. Total Eubacteria 16S rDNA was served as an internal control.

Administration of drugs to SPF mice

After ABX administration, mice underwent bacterium and metabolite treatment. For bacterium treatment, the mice were gavaged with a bacterium or culture medium three times a week for 4 or 6 weeks beginning the following day. For metabolite treatment, the ABX treated mice were gavaged or intraperitoneally injected with PC (20 μM), intraperitoneally injected LPC (20 μM) or the same volume of 1xPBS three times a week for 4 or 6 weeks. For drug administration, the mice were intraperitoneally injected with liproxstatin-1 (10 mg/kg) or orally administered with APD668 (10 mg/kg) every two days for a continuous period of 30 days.

Preparation of mouse tissue samples

To prepare tissue samples for RNA extraction, protein isolation, flow cytology and single cell separation, histology, and transmission electron microscopy (TEM), mice were first deeply anesthetized by IP injection of tribromoethanol (125–250 mg/kg). For RNA extraction, brains of mice were rapidly dissociated on ice, then the hippocampi were directly frozen in 600 μl TRIzol and stored at -80°C refrigerator. In order to extract protein, brains of mice were promptly dissected on ice, the hippocampi were isolated and rapidly frozen using EP tubes in liquid nitrogen, and then stored at -80°C. For flow cytometry and single cell separation, after anesthetizing the mice, they were perfused with cold PBS through the left heart to reduce the interference of red blood cells, and

hippocampus were digested immediately. For histology, anesthetized mice were transcardially perfused using cold 1xPBS and 4% paraformaldehyde (PFA). The collected brain tissues were postfixed in 4% PFA at 4°C overnight. For TEM, anesthetized mice were perfused with 40ml 1x PBS and then perfused with 40 ml of a solution with a concentration of 4% PFA and 1% glutaraldehyde. About 1 mm^3 brain tissue separated from the hippocampal subiculum were promptly placed in the 1% glutaraldehyde and store at 4°C.

Immunofluorescence

After PFA fixation, brains were treated by sequential equilibration in 15% and 30% sucrose in 1x PBS for 24 h respectively. Then, the dehydrated brains were immersed in Tissue-Tek OCT compound for embedding. Serial coronal brain sections with a thickness of 40 μm were generated using a sliding, freezing microtome (Leica Microsystems). After washing the sections with PBS for 3 times, tissues were permeabilizated using a solution of 0.3% Triton X-100 for 20 minutes, followed by blocking with 2% bovine serum albumin (BSA) for a duration of 1 hour. Then the sections were incubated with anti-6E10 (1:500), anti-Aβ (1:1000), anti-Iba1 (1:1000), anti-GFAP (1:100) and anti-LAMP1 (1:200) antibodies for 16 h at 4°C. The next day, the sections were underwent incubation with secondary antibodies that were conjugated with Alexa Fluor 488- and 594 for a duration of 90 minutes at room temperature. Finally, the nuclei were labeled with 4',6-diamidino-2-phenylindole (DAPI) for a period of 20 min at ambient temperature. Images were captured using a confocal microscope (Olympus, FV3000). The load of Aβ plaque and the density of Iba1- and GFAP-immunoreactive cells were quantified by ImageJ software.

NOR test

The NOR test was performed as previously described.[60] Mice were allowed to acclimate in the experimental room for a minimum of 30 minutes, then tested within a designated chamber (a 25 × 25 × 25 cm white acrylic box). The chamber comprised two identical objects (referred to as the old objects). The mice were placed faced away from the object inside a chamber and given a 10-minute period for free exploration, followed by putting them to home cages for an interval of 1 h. During the testing session, one of the objects was substituted with a new object, and the mice were given 5-minute to explore. After each trial, the chamber and objects were cleaned with 75% alcohol. The videos were recorded using a camera and subsequently analyzed through manual timing in a blinded fashion. The time spent exploring each object was assessed when the mouse sniffed or touched the object within a 2 cm range while visually attending to it. Instances where the mouse sat near the objects, climbed on them, or chewed them were excluded. The novel object recognition index was computed by dividing the time animal explored the new object by the total time that the mouse explored with two objects.

MWM test

The MWM test was conducted following the established protocol as previously described.[61] During the training phase, mice were placed in a pool filled with opaque water with a temperature of 21-23°C. Mice underwent a total of four trials every day for five consecutive days. The mice were permitted to swim until they located the platform and were required to remain on the it for at least 15 seconds. If a mouse was unable to locate the platform within 90 seconds, the experimenter would guide it to the platform. The time gap between each trial was no less than 1 minute. After 5 days of training, probe test was conducted on the next day. On that day, the platform in the water was removed, and the percentage of time spent in the target quadrant for a 60-second duration was calculated. Tracking Master software and Panlab SMART video tracking system (Smart 3.0) were used for video recording and data analysis.

CFC test

During the training phase, the mouse was introduced to a white soundproof cubicle (chamber A), which had a metal wire floor, an opaque triangular ceiling and 5% acetic acid. The activity during at first 3 minutes was measured as baseline activity. After that, a continuous tone with a frequency of 4000 Hz and a sound level of 80 dB was presented as a conditioned stimulus (CS). During the last 2 seconds of the CS period, a continuous foot shock with an intensity of 0.6 mA was delivered as an unconditioned stimulus (US) to the mouse. This CS-US pairing was repeated 3 times, with a 60-second break between each trial. After the final shock, the mouse was kept in the chamber for an additional 1 minute. The next day, mice were exposed to the chamber A for 3 min without a foot shock to assess the conditioned freezing (context). The cued test was performed on the third day. The chamber was replaced with a smooth floor and a nontriangular ceiling, but without acetic acid. The first 3 minutes were recorded as baseline activity, after which the mice were exposed to the same tone as presented in chamber A without foot shocks. After each training or testing session, using 75% alcohol to sanitize chambers. Using cameras with an automated analysis system to record and analyse freezing time (VideoFreeze™ Video Fear Conditioning Software).

Slice preparation and electrophysiological recordings

The brains of six-month-old mice were removed and placed in cold dissection buffer as previously reported.[62] Using a vibrating microtome (VT-1200s, Leica) to prepare 400 μm thick horizontal hippocampal slices. The slices were then incubated in artificial cerebrospinal fluid (ACSF) and bubbled with 95% O_2 and 5% CO_2 for 1 hour at room temperature. The formula of ACSF and the recording and analysis methods of long-term potentiation (LTP) are described in the previous literature.[63]

TEM

After washing the fixed tissues with phosphate buffer (PB) and deionized water, the tissues were soaked in a ferricyanide aqueous solution containing 1% OsO4 and 1.5% potassium for 2 hours at 4°C. Then, the tissues were washed and dehydrated. Samlpes were then infiltrated with a mixture of acetone and SPI-PON812 resin, and finally transferred to pure resin. After embedding samples in pure resin with 1.5% BDMA, they were polymerized for 12 hours at 45°C and 48 hours at 60°C. Finally, the ultrathin sections were made with a precise thickness of 70 nm and double-stained using uranyl acetate and lead citrate. Subsequently, the sections were observed with a transmission electron microscope (FEI Tecnai Spirit120kV).

Untargeted metabolomics

Metabolite extraction and detection were performed at Novogene Co., Ltd. (Beijing, China). The serum samples were added with prechilled 80% methanol and mixed by vortexing. The supernatant was collected by centrifugation. Afterwards, the methanol was diluted to a concentration of 53% using water, and the mixture was centrifuged once again, followed by the collection of the supernatant for UHPLC–MS/MS analysis. Using a Hypesil Gold column, the sample flow rate was 0.2 mL/min. Eluent A were 0.1% FA (positive mode) or 5 mM ammonium acetate (negative mode) and Eluent B is methanol. Solvent gradient was programmed from 2% B for 1.5 minutes, followed by 2%-100% B for 3 minutes. Then, mobile phase was held at 100% B for 10 minutes, followed by 100%-2% B for 10.1 minutes. Finally, the mobile phase was held at 2% B for 12 minutes. The mass spectrometer was set a voltage of 3.5 kV, a sheath gas flow rate of 35 psi, a capillary temperature of 320°C, an S-lens RF level of 60, an auxiliary gas flow rate of 10 L/min, and an auxiliary gas heater temperature of 350°C.

Metabolites which had a Variable Importance in Projection (VIP) value greater than 1 and P-value less than 0.05, and fold change (FC) $\geq$ 2 or FC $\leq$ 0.5 were considered as differential metabolites. The metaX software was utilized to conduct Principal components analysis (PCA). Volcano plots was generated using the R language package "ggplot2" in, The R language package "pheatmap" was used to generate clustering heatmaps.

UPLC-MS and Lipidomics

The content of PC, LPC and APD668 in multiple samples was detected by UPLC-MS. For serum from mice or human patients, 150 μl of precooled (-80°C) methanol was added to 50 μl of serum. After incubating samples on ice for 5 minutes, they were centrifuged at 4°C, 15,000 ×g for 20 minutes. 100 μl of the supernatant was absorbed and dried under nitrogen gas. Then, the samples were re-suspended in 500 μl of methanol and detected. For PC degradation by bacteria, indicated strains were cultivated to an OD600 of 1.0. PC was added to the culture strains at a final concentration of 1 μg/ml. After centrifugation at 5000 rpm at 4 °C for 10 min, the supernatants were collected for further detect. The APD668 in the brain was detected by grinding the whole brain tissue in liquid nitrogen. Then, 100 mg of the resulting powder was weighed and mixed with 5 times the volume of methanol. The mixture was centrifuged at 4°C, 15,000 ×g for 20 minutes. The supernatant was collected for further analysis. For the lipidomics analysis of the ferroptotic lipid signature, after grinding the hippocampal tissue in liquid nitrogen, 50mg of powder was accurately weighed. Then, lipids were extracted using the Folch procedure with the addition of 0.01% butylated hydroxytoluene (BHT). 16:0-18:1 PE-d_{31}(5 μg/mL) was used as an internal standard. In Acquity I-Class ultrahigh-performance liquid chromatography system, C18 column was used, column temperature was 50°C and flow rate was 0.3 mL/minute. Using 60/40 (v/v) acetonitrile/water as eluent A and 90/10 (v/v) isopropanol/acetonitrile as eluent B. Solvent gradient was performed as following: 0-2.5 minutes 30% B, 2.5-8 minutes 50% B, 8-10 minutes 98% B, 10-15 minutes 98% B, 15-18 minutes 30% B. In mass spectrometer (Waters Vion-IMS-QToF), the voltage was 2.5 kV, the scan time was 0.1 s, gas flow wad 800 L per hour, and collision energy (MSE) was from 20.00 eV and to 30.00 eV. LPC and PC were used as standards and detected in negative ion mode. For lipidomics, metabolites with mass ranging from 50 to 1000 m/z were detected in both negative and positive ion mode. The data were analyzed using UNIFI 1.9.3 software. 3D peak detection was used to evaluate deconvolution and peak picking.

Metabolomic and metagenomic data correlation analysis

A correlation analysis was performed between metagenomic and metabolomic, focusing on genomes and metabolites that were identified as significantly different between 5xFAD mice and age-matched WT mice. The genome relative abundance and raw metabolite values were log-transformed, and Spearman's correlation coefficients assessment was conducted using R version 4.1.2. The different species and metabolites with over two-fold changes between the two groups, with a correlation coefficient greater or equal to 1 and P-value < 0.05, were also analyzed.

Single-cell sorting

The single-cell suspensions of hippocampi were prepared using the Adult Brain Dissociation Kit. According to the manufacturer's instructions, the tissues were enzymatically and mechanically dissociated combine components of the kit with a gentleMACS™ Dissociator with Heaters. Following dissociation, debris was eliminated using Debris Removal Solution. The resulting single-cell suspensions were labeled with Mouse Adult Neuron Isolation Kit, anti-O4 MicroBeads, CD11b (microglia) MicroBeads and anti-ACSA-2 MicroBeads at the dilution suggested. Neuron, oligodendrocytes, microglia and astrocyte cells were isolated using LS columns (Miltenyi Biotec) and a MACS MultiStand Separator (Miltenyi Biotec).

Please cite this article in press as: Zha et al., Microbiota-derived lysophosphatidylcholine alleviates Alzheimer's disease pathology via suppressing ferroptosis, Cell Metabolism (2024), https://doi.org/10.1016/j.cmet.2024.10.006

Single-cell sequencing (Smart-seq2)

The cell suspensions were diluted and aliquoted through 384-well plates to ICELL8 350v chips (Clontech). Using the ICELL8 cx Single-Cell System (Takara) and CellSelect software, the nanowells on the chip were imaged and selected manually. Follow the provided instructions to proceed with the subsequent DNA synthesis process. Briefly, Using SMART-Seq ICELL8 CDS as an oligo dT primer to synthesize the first-strand cDNA. Then the template was switched at the 5′ end by SMART-Seq ICELL8 Oligonucleotide. Full-length cDNA was amplified and tagmented. Then, the tagmented DNA was amplified using the "Library PCR 1 program". Subsequently, the library was extracted from the chip and purified with AMPure XP beads at a ratio of 1:1. Finally, a sequencing-ready library was prepared with the "Library PCR 2 program" and purified using AMPure XP beads. After assessing the library size distribution and quantification, the library was sequenced using an Illumina Nextera instrument.

Smart-seq2 data processing

The reads from the Smart-seq2 data were aligned to the UCSC mm10 mouse genome reference with STAR (version 2.7.9a). Conducting downstream analyses using the R package Seurat (version 3.1.0). The ReadSTARSolo function was used to import the matrix of gene-level counts. Using the NormalizeData function, the cell counts were normalized, ensuring that the total count per cell was 10,000. Uniform manifold approximation and projection (UMAP) was used for dimensionality reduction, then visualization of the data. Wilcoxon rank sum test were used to identify differential expression, and the identify of unique expression profiles were performed between clusters and genotypes.

Quantitative reverse transcription PCR

Total RNA was extracted from hippocampus of the mice and cultured cells using RNA isolation kit. Then the first strand cDNA was synthesized by HiScript II One Step RT-PCR Kit. The PowerUp SYBR Green Master Mix was used to conducted the real-time PCR. The ABI StepOne Plus instrument was used to run the program. The threshold cycle (Ct) value of each gene was normalized to that of β-actin for quantification. The $2^{-\Delta\Delta Ct}$ method was utilized for analysis.

Western blot assay

The hippocampus and cultured cell samples were lysed by RIPA supplemented with PMSF and Complete Proteaseprotease Inhibitor. The lysates were then homogenized using FastPrep-24 (MP Biomedicals) and kept on ice for 40 minutes. The supernatant was collected after being centrifuged at 4°C, 15000 xg for 20 min, then denatured with loading buffer at 95°C for 10 minutes. Protein amounts of 20-30 μg of were loaded on 12.5% SDS-PAGE gels and run at 80V for 30 minutes followed by 120V for 60 minutes. The proteins were then transferred from the gel onto a PVDF membrane using eBlot™ L1 instrument. The membrane was subsequently blocked with 10% nonfat milk for 1 hour then incubated with antibodies at 4°C overnight. The following antibodies were used: anti-GPX4 (1:1000), anti-FACL4 (1:1000), anti-NRF2 (1:1000), anti-FSP1 (1:1000), anti-MBOAT1 (1:1000), anti-LC3 (1:1000), anti-MBOPB (1:1000) and anti-actin (1:2000). The following day, the membrane was incubated with secondary antibody then scanned with an infrared fluorescence scanning imaging system (Odyssey). The expression level of the target band, relative to that of actin, was quantified with ImageJ software.

Malondialdehyde (MDA) content

The MDA content in the hippocampus of mice was measured with the Lipid Peroxidation (MDA) Assay Kit following the protocols. In brief, fresh hippocampal tissues were weighed, lysed using MDA lysis buffer added with butylated hydroxytoluene (BHT) and centrifuged. The supernatant was mixed with thiobarbituric acid (TBA) then incubated at 95°C for 60 minutes. After cooling on ice for 10 minutes, the absorbance of the TBA-reactive substances was measured at 532 nm using spectrophotometer. Calculating MDA in nmol/mg tissue to quantify lipid peroxidation.

Cell lines and culture conditions

BV2 and SH-SY5Y cells were purchased from ATCC, HT22 cells were obtained from Ubigene (Guangzhou, China). Cells were cultured in DMEM supplemented with 10% FBS and 1% penicillin/streptomycin and incubated at 37°C in a humidified atmosphere with 5% CO_2.

Knockout and overexpression of target genes

The genes of ACSL4, GPR119, GPX4, and NRF2 were knocked out using the CRISPR/Cas9 system. Single sgRNA guides were designed to target critical exons of these genes to for inactivation. The guides were cloned into the YKO-LV001-single-gRNA vector. Lentiviruses were prepared by Ubigene (Guangzhou, China). SH-SY5Y-Cas9 and BV2-Cas9 cells were generated by transducing SH-SY5Y and BV2 cells with YCas-LV001 lentiviral particles, followed by selection using puromycin. Then the Cas9 cells were seeded onto 12-well plate and co-transfected with the desired sgRNA-expressing plasmid. The single cell clones were picked, and knockout clones were identified by sequencing. Lentiviruses for ACSL4 overexpression were prepared by GenePharma (Shanghai, China). BV2 and SH-SY5Y cells were transducted with lentivirus particles of ACSL4 in a 6-well plate, incubated in a CO2 incubator for 72 hours to establish stable cell lines.

Cell ferroptosis treatment and assessment

HT22, SH-SY5Y and BV2 cells were seeded in 96-well plates or 12-well dishes one day prior to the experiment. The following day, HT22 cells were treated with RSL3 at a concentration of 0.5 μM or erastin at a concentration of 1 μM, while SH-SY5Y and BV2 cell were treated with RSL3 at a concentration of 7 μM to induce ferroptosis. Correspondingly, 500 nM LPC, 200 nM APD668 or 1.25 μM Lip-1 were added to the indicated wells for a duration of 20 hours. Control groups were treated with DMSO and PBS. Then cell viability was assessed using the alamarBlue as an indicator. Cell death was evaluated by measuring LDH release using Cytotoxicity Assay Kit following the manufacturer's instructions.

Flow cytometry

Single-cell suspensions of hippocampi were prepared using the Adult Brain Dissociation Kit. Flow cytometry was used to assess ROS and lipid peroxidation in living hippocampal cells of 5xFAD mice and cells from various treatment groups. For cell suspension of mice, cells were incubated with Zombie Yellow solution (1:100) for 20 min at room temperature. Following a wash with Cell Staining Buffer, 10 μM CellROX™ Green or 5 μM C11-BODIPY (581/591) were used to incubate with cells at 37 °C for 30 min prevent exposure to light. After washing 3 times with PBS, the cells were resuspended in 300 μL of PBS containing 1% BSA for detection. For ferroptosis treated cells, at the last 30 min of treatment, cells were incubated with 5 μM of CellROX Green or C11-BODIPY (581/591) resuspended in culture medium. As for SPY-LHP oxidation, cells were cultured with 5 μM of SPY-LHP for 30 minutes at incubator after seeding for 12 hours, then cells were washed with DMEM and treated to induce ferroptosis. Before harvesting by trypsinization, cells were washed with PBS. Cells were then resuspended in 300 μL of PBS and analyzed using a flow cytometer (LSRFortessa, BD Biosciences). The obtained data were analyzed using the FlowJo Software.

FMT experiments

Fresh feces were collected from mice and a suspension was prepared by adding 3 ml of sterile PBS per 10 fecal pellets. Thoroughly crush the fecal pellets to achieve a homogeneous suspension. Then, settle the suspension for a few minutes to allow the fragments to sediment. Transfer 200 μL of the suspension into each ABX-pretreated recipient using oral gavage three times per week for a duration of 4 weeks.

Egg yolk agar plate assay for phospholipase activity

The biological activity of *B. ovatus* and recombinant *E. coli-pla2* were assessed using the egg yolk agar plate. The plate containing 1.09% boric acid, 0.19% borax, 0.66% NaCl, 2% agar, and 4% egg yolk salt solution. A drop of a bacteria suspension (approximately 20 microliters) was placed on the surface of egg-yolk agar plate. The plates were then incubated at 37 °C, after 24 hours of incubation, the formation of precipitation zones was examined.

Expression of phospholipase A2 in *E. coli*

PLA2 was amplified by PCR from the chromosomal DNA of *B. ovatus* using the primers (PLA2F:5'-GCGAATTCACGACTAAGACT GAG-3', PLA2R: 5'-GCGAATTCGACACGAAAGTCCTC-3'). The EcoRI restriction site, which was used for subsequent cloning, is underlined. The PCR product was digested with EcoRI and ligated into the pET-21b (+) vector using T4 ligase. Subsequently, the vector pET-21b (+) -PLA2 was introduced into *E. coli* BL21 (DE3) by heat shock transformation. After transformation, LB agar plates containing ampicillin were used to select positive transformants, which were designated as *E. coli*-PLA2. *E. coli* carrying the empty vector served as the negative control. To expression PLA2 in *E. coli*, fresh LB broth containing with ampicillin was inoculated with a 1% v/v overnight cultured *E. coli*-PLA2. After cell density reached to OD600 nm of 0.6, IPTG was added to a final concentration of 0.5 mM to induce the expression of the fusion protein for 6 h at 37 °C. The cell pellets were harvested by centrifugation at 5000 rpm for 5 min.

RNA-sequencing

The total RNA from ferroptosis induced cell was extracted and underwent the quality control procedures. RNA sequencing library was prepared by Novogene Co., Ltd. (Beijing, China). mRNA was purified and fragmented, followed by the synthesis of the first strand cDNA. Then dNTPs and DNA polymerase I were added to initiate the synthesis of the second strand. Then the DNA underwent terminal repaired and was ligated with sequencing adaptors. The cDNA library was made through size selection and PCR enrichment. The qualified libraries were loaded onto Illumina Novaseq6000 sequencers to collect paired-end reads.

QUANTIFICATION AND STATISTICAL ANALYSIS

Data were shown as mean ± SEM. Data points of individual observations were displayed. Statistical analyses of the data were performed using GraphPad Prism 8.0. Differences between groups were assessed using either one- or two-way analysis of variance (ANOVA) and unpaired Student's t-test. Statistical tests used for group or cluster comparisons in metagenomics, metabolomics, metagenome-metabolome correlation, single-cell RNA-seq experiment analysis were specified in the respective sections in methods. A P value < 0.05 was considered statistically significance for all data sets. P values were represented on figures as follows: ns, not significant, *$p < 0.05$, **$p < 0.01$, ***$p < 0.005$, ****$p < 0.001$. Each experiment was repeated independently for at least three times.